THESIS

RESPONSE OF MCSs AND LOW-FREQUENCY GRAVITY WAVES TO VERTICAL WIND SHEAR AND NOCTURNAL THERMODYNAMIC ENVIRONMENTS

Submitted by

Faith Groff

Department of Atmospheric Science

In partial fulfillment of the requirements

For the Degree of Master of Science

Colorado State University

Fort Collins, Colorado

Fall 2019

Master's Committee:

Advisor: Russ S. Schumacher
Co-Advisor: Rebecca D. Adams-Selin

Kristen L. Rasmussen
Peter A. Nelson

ABSTRACT

RESPONSE OF MCSs AND LOW-FREQUENCY GRAVITY WAVES TO VERTICAL WIND SHEAR AND NOCTURNAL THERMODYNAMIC ENVIRONMENTS

Low-frequency gravity waves have been found to both increase and decrease environmental favorability ahead of mesoscale convective systems (MCSs) based on their associated vertical motions. The strength and timing of these waves is determined by the internal dynamics of the MCS. This study investigates the sensitivities of MCSs to changes in the vertical wind and thermodynamic profiles through idealized cloud model simulations, highlighting how internal MCS processes impact low-frequency gravity wave generation, propagation and environmental influence. A common feature among all of the simulations is that fluctuations within the internal latent heating profile, the generation mechanism behind n = 1 (N1) waves, display concurrent cellularity with the MCS updrafts. Spectral analysis is performed on the rates of latent heat release, updraft velocity, and deep-tropospheric descent ahead of the convection as a signal for N1 wave passage. Results strongly suggest that perturbations in mid-level descent up to 100 km ahead of the MCS occur at the same frequency as N1 gravity wave generation due to fluctuations of latent heat release caused by the cellular variations of MCS updrafts. The introduction of deep vertical wind shear does not change this connection nor impact the lifecycle of daytime MCS updrafts and associated N1 wave generation, however within a nocturnal environment, the frequency of the cellularity of the updrafts increases, subsequently increasing the frequency of N1 wave generation.

In response to surges of latent cooling within the lower half of the troposphere, n = 2 (N2) low-frequency gravity waves are generated, however this only occurs with cooling contributions from both evaporation and melting of hydrometeors. Results indicate that in environments with minimal upper-level wind shear atop more pronounced shear below, the N2 wave generation mechanisms and environmental influence behave similarly among daytime and nocturnal MCSs. Within environments that incorporate deep vertical wind shear, many of the N2 waves are strong enough to support cloud development ahead of the MCS as well as sustain and support convection within the domain.

ACKNOWLEDGMENTS

This research was supported by the National Science Foundation Grants AGS-1636663 and AGS-1636667. High-performance computing support from Cheyenne (doi:10.5065/D6RX99HX) was provided by NCAR's Computational and Information Systems Laboratory, sponsored by the National Science Foundation. The author also thanks Dr. Elizabeth Barnes for her guidance on statistical analysis used in this research.

DEDICATION

This research is dedicated to Nancy Plunkett, who never stopped learning and always encouraged others to do the same.

TABLE OF CONTENTS

CHAPTER 1

INTRODUCTION

On the night of 14-15 July 2015, the Plains Elevated Convection at Night (PECAN) field campaign embarked on a convection initiation (CI) mission in eastern Colorado. The convection quickly organized into a mesoscale convective system (MCS) and marched through Kansas with the leading convective line extending through Nebraska and a rapidly developing stratiform region trailing behind. As the storm began to bow and the stratiform region widened, a radar fine line (a signal of convective outflow often indicative of bores and gravity waves) swiftly propagated away from the MCS and passed through the observational network in Hastings, Nebraska, later initiating an arc of convection far removed from the MCS itself. MCSs can generate numerous kinds of waves, bores, and outflows that may lead to new convection initiation if not, at the very least, work in concert to alter the downstream environment. A study of another PECAN case attributed CI to gravity waves that had propagated over 100 km away from their source and acted to lift parcels to their level of free convection (LFC; Wilson et al. 2018). The motivation behind this thesis is to develop a better understanding of low-frequency gravity wave generation mechanisms and propagation, particularly in realistic nocturnal environments favorable for MCS development and sustainability, as well as their subsequent downstream environmental adjustments that can act to support or suppress potential CI.

A general qualifying characteristic for a storm system to be classified as a MCS is that it must have a precipitation region extending over 100 km or more, often partitioned by distinct regions of convective and stratiform precipitation as can be seen on radar (Houze 2004). The convective region consists of numerous deep cells of high reflectivity accompanied by individual updrafts that generate immense amounts of diabatic heating due to the formation of condensate resulting in net heating at all vertical levels with a maximum in the mid-levels (e.g. Gallus and Johnson 1991; Nicholls et al. 1991; Houze 2004). The stratiform region, composed of lighter, more consistent precipitation, includes old cells from the convective line that have been advected upstream due to the front-to-rear ascent characteristic of these systems (Houze 2004). While the upper levels of this region are still dominated by latent heating, cooling prevails in the lower half due to the expansive evaporation and melting of hydrometeors.

The latent heating profiles can be classified by the number of tropospheric antinodes in each profile. The wavelength of the convective heating profile is twice the depth of the troposphere (one antinode) as it has an entirely positive heating component maximized in the midlevels. The wavelength of the stratiform region heating profile is the depth of the troposphere as it has two antinodes, one in the lower levels reflecting latent cooling and another elevated antinode for warming. A schematic of the individual convective and stratiform vertical heating profiles can be seen in Fig. 1.1 (a). The net heating profiles between the two regions as a function of varying stratiform extent are shown in Fig. 1.1 (b). Houze (2004) remarked that as the stratiform precipitation region expands, the heating maximum becomes increasingly constricted yet elevated, indicating that the vertical heating structure of a MCS shows a reliance on the expanse of the stratiform region in reference to the whole system.

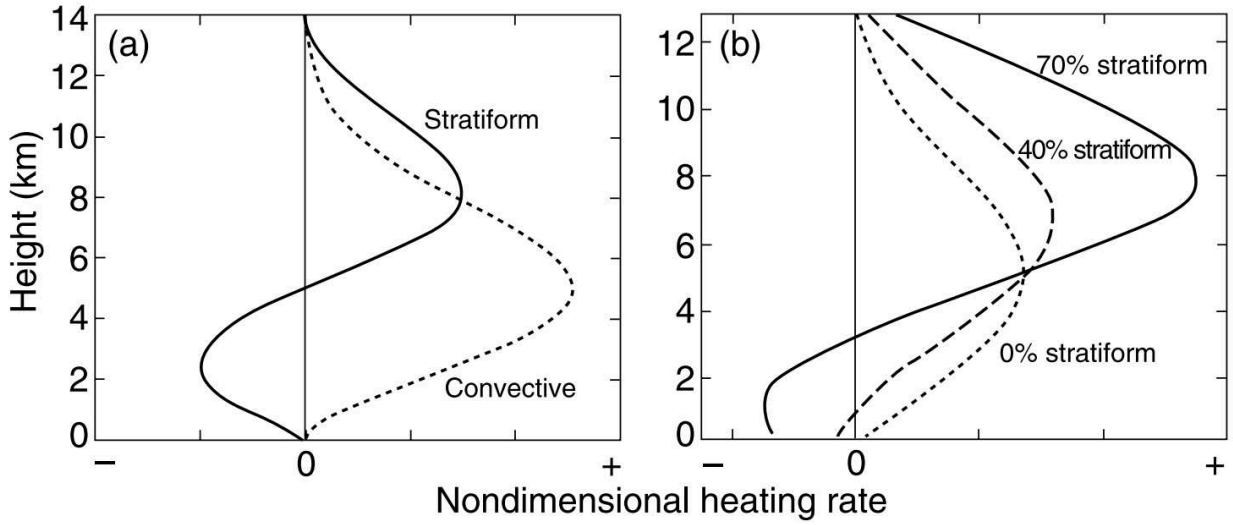

FIG. 1.1. (a) Vertical heating profiles within MCS precipitation regions, where the dashed line shows the heating profile for the convective region and the solid line the stratiform. The net heating profiles for the entire MCS are shown in (b) based on different ratios of stratiform precipitation. Figure 4 from Houze (2004).

This onset of mass amounts of latent heat release throughout the depth of the troposphere causes a gradient between the buoyancy within the convective system and surrounding stratified environment. In response, nearly hydrostatic and quasi linear low-frequency gravity waves act to neutralize this imbalance through distribution of momentum (Schmidt and Cotton 1990; Houze 2004; Fovell et al. 2006; Adams-Selin and Johnson 2013). These waves are manifested over an expansive distribution of length and time scales and are defined by the number of antinodes within the latent heating profile that ignited them. A profile for the convective region, as seen by the dashed line in Fig. 1.1 (a), would be

defined as an n = 1 (hereafter N1) wave due to heating at all levels, and the stratiform region, represented by the solid line, would be defined as an n = 2 (hereafter N2) wave for the maximum in cooling in the lower levels and maximum in heating in the upper levels.

These waves are able to propagate primarily horizontally without the necessity of trapping or ducting (Nicholls et al. 1991; Pandya et al. 1993; Mapes 1993; Fovell et al. 2006; Lane and Zhang 2011). Lane and Reeder (2001) reiterated this point. They demonstrated that the speed of any vertical wave propagation would be sufficiently smaller than the speed of horizontal propagation, and because the wave's horizontal wavelength is considerably larger than the vertical wavelength, the angle at which they travel would be almost parallel to the horizontal. Nicholls et al. (1991) found that the wave speed under these conditions is

$$c = \frac{NH}{n\pi} \tag{1.1}$$

c being the gravity wave speed in m s^{-1}, N the Brunt-Väisälä frequency in s^{-1}, H the height of the tropopause in meters, and n the number of antinodes in vertical heating profile within the MCS at time of generation. The larger wavelength of N1 waves means that they will travel at twice the speed of N2 waves.

Numerous studies have been performed to understand the surrounding environmental impact that the latent heating profiles within MCSs and subsequent gravity wave propagation may cause. By introducing an uninterrupted heat source representative of the convective latent heating profile as seen in Fig. 1.1 (a), Nicholls et al. (1991) was able to analytically calculate the linear solutions of the hydrostatic Boussinesq equations to articulate how N1 waves may manifest themselves downstream. Through their various tests, they consistently found that this heating profile induced deep-tropospheric descent at the wave front and subsequent adiabatic warming of the column as the wave propagated away from the system as seen in Fig. 1.2 (a). In another simulation, when the heating was eventually turned off, a wave of the same vertical extent was generated that had deep-tropospheric ascent, implying the ability of N1 waves to have an updraft/downdraft couplet. The same simplified model was used to calculate the environmental response to N2 waves by introducing a steady-state profile of the stratiform region. This profile produced a wave that had ascent through the bottom half of the troposphere topped by descent in the upper half, promoting adiabatic cooling and warming respectively. They found these wave responses similar to a gravity wave produced in a numerical simulation of convection in Florida.

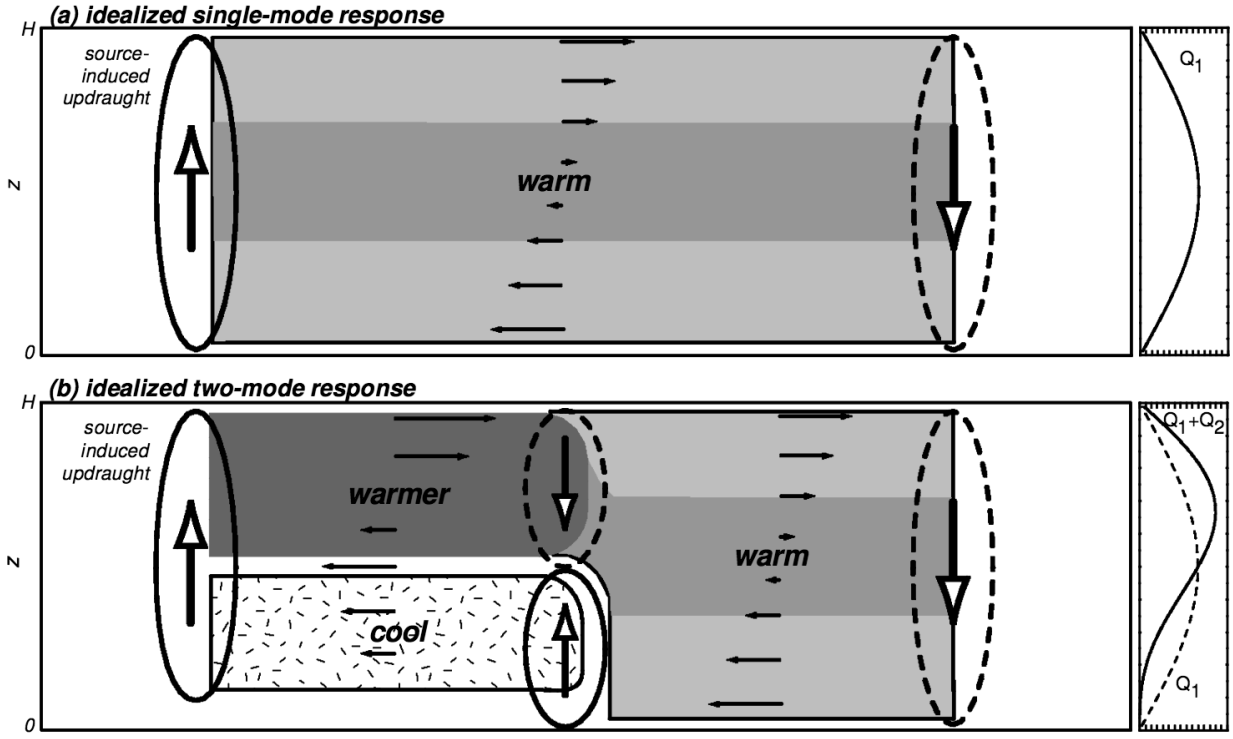

FIG. 1.2. Downstream response to sustained vertical heating profiles, shown in the right panels, that generate (a) an N1 wave and (b) an N2 wave following an N1 wave. Upward motion is indicated by the solid ovals and descent by the dashed ovals. The horizontal black arrows show zonal wind where the N1 wave induces inflow in the lower levels and outflow in the upper levels, while the N2 wave increases mid-level inflow and supports outflow in the upper and lower levels. Figure 11 (a) and (b) from Fovell (2002).

Mapes (1993) built upon the same simplified model used in Nicholls et al. (1991), but tested instead a combination of the N1 and N2 latent heating profiles, arguing that this kind of profile was more representative of the latent heating structure within an MCS. Similarly, the study introduced a constant heat source, but the structure now included contributions of latent heating from the stratiform region as well as evaporational cooling from the convective downdrafts. This model showed similar environmental responses to N1 and N2 waves downstream, but instead of seeing these waves in individual tests, both waves were observed in one simulation due to this combined heating profile shown in the right panel of Fig. 1.2 (b).

Mapes previously stated that the constant heat source of the N1 profile would generate a wave that would permanently alter the environment conditional upon the absence of another wave passage. The N1 wave and associated descent and warming increased the stabilization of the forward environment,

suppressing new convection. However, this influence can be negated and even surpassed with the passage of an N2 wave. The peak descent and therefore warming from N1 waves occurs in the middle of the troposphere, however the adiabatic cooling and ascent associated with N2 waves show maximums in the lower levels, playing a critical influence in destabilizing the environment and increasing the convective available potential energy (CAPE). While this influence is seen near the MCS, the environmental adjustments to these waves are recognized far beyond the MCS outflow. Mapes found that even if the ascent is not enough to lift parcels to their LFC, the destabilization that N2 waves offer nonetheless provides a favorable environment for CI.

McAnelly et al. (1997) used the same model to test pulses of the N1 and N2 generation profiles. The N1 heating source produced the same deep-tropospheric subsidence, however once the heating tapered, a subsequent updraft couplet was produced to the downdraft portion of the wave. Their study found that at most this updraft could act to negate the influence of the downdraft portion, but that it would not increase favorability beyond the original conditions. Following this initial heat burst, the N2 generation structure was superimposed on the prescribed vertical profile, where the cooling in the lower levels and heating in the upper levels created a profile with zero net heating. The ascent from these waves acted to increase CAPE while simultaneously decreasing convective inhibition (CIN) particularly close to the MCS proxy, adding instability to the immediate environment and potentially promoting CI downstream. The storm inflow can also advect this favorable air into the MCS.

These studies laid the foundation for deep-tropospheric, low-frequency gravity wave generation, propagation, and environmental influence, however the simplified hydrostatic model lacks key features of realistic environments to truly represent all the aspects of these waves. Nicholls et al. (1991) remarked on their own model that using a prescribed heat source to represent an MCS has considerable flaws as the nonlinear and non-hydrostatic processes within convection certainly have an impactful influence on the vertical heating structure. These simulations also did not include any background flow and were calculated for an infinitely expansive fluid, further lacking the representation of an authentic downstream environment.

Studies performed after these have continued to develop the understanding of low-frequency gravity waves through inclusiveness of realistic MCS and environmental processes by examining them in increasingly advanced model simulations as well as analyzing them in observations. Replacing prescribed heat sources, cloud resolving models as well as numerical simulations have reiterated many of the same conclusions from previous works. All the studies agree that the response to deep convective

heating within an MCS is a fast moving wave of tropospheric descent that acts to warm the column and suppress new convection by increasing stability for large distances past the MCS (e.g. Lane and Reeder 2001; Fovell 2002; Fovell et al. 2006). Secondly, when cooling is introduced in the lower-levels, a wave characteristic of ascent through the lower half of the troposphere propagates away from the MCS and acts to decrease stability through adiabatic cooling, increasing the relative humidity of a now lifted layer (e.g. Fovell et al. 2006; Lane and Zhang 2011; Adams-Selin and Johnson 2013; Adams-Selin 2019).

Further inquiries into the propagation and environmental influence of low-frequency gravity waves have emphasized the importance they can have in increasing or decreasing environmental favorability. This can have an impactful influence on the parent MCS, potentially acting to sustain and support the MCS but also promote CI downstream. Lane and Reeder (2001) used a cloud-resolving model that included moisture and allowed thermodynamic processes under the argument that condensational heating within the updrafts influences the internal heating profile, a process not permitted or observed in the previous linear models. This study applied the understanding of low-frequency gravity wave generation and propagation to a single tropical convective cloud and found that the waves display similar behavior to the waves in the linear models. They found that the subsidence warming from the passage of an N1 wave acts to decrease CAPE while an N2 wave acts to increase it. Furthermore, N2 waves also have a greater influence on CIN as the ascent and associated cooling has more influence near cloud base than N1 waves. These results were also echoed in Adams-Selin and Johnson (2013) and Adams-Selin (2019) through observations and Cloud Model 1 (CM1) simulations.

Fovell (2002) and Fovell et al. (2006), using a parameterized nonlinear and non-hydrostatic cloud model and numerical simulations respectively, highlighted the importance of the nearly saturated layer that an N2 wave can create and elongate ahead of an MCS. The low-level ascent causes adiabatic cooling of a layer that can aid in bringing it closer to saturation and decrease static stability. While N2 waves can act to establish this moist layer, high-frequency waves can then serve as the catalyst for CI within this layer. If these cells become absorbed by the MCS, it can lead to discrete propagation of the system in which it rapidly increases in speed. This moist layer and additional N2 wave processes can also help to sustain or even strengthen the MCS. Building upon the broad statements of MCS reinvigoration by the processes of N2 waves in Mapes (1993) and McAnelly et al. (1997), Adams-Selin and Johnson (2013) directly connected how the increased CAPE within this sub-saturated layer becomes part of the inflow to the MCS and can strengthen the convective updrafts. This positive feedback from layers influenced by an N2 wave passage and intensification of the parent system are also seen in single

convective clouds in Lane and Zhang (2011) as well as supercells in Trapp and Woznicki (2017). These advancements within gravity wave intelligence have actively increased our understanding between an important feedback system as well as environmental modification particularly within tropical convection and daytime MCS environments.

Recent studies have begun to explore the prospect and influence of multiple low-frequency gravity waves being generated within one convective system. Adams-Selin and Johnson (2013) observed multiple N1 waves within observations as well as the cloud model simulation of the same event, attributing each wave to changes within the vertical heating profile. Adams-Selin (2019) built upon this theory by connecting changes in the heating profile and subsequent gravity wave generation to updraft periodicity, an idea first proposed by Nicholls et al. (1991) discussing how the heating structure within an MCS is likely coupled to the vertical velocity. These studies suggest that N1 gravity wave generation can be intricately linked to the characteristic cellularity of MCSs, a process also noted of convective cloud fields in Lane and Zhang (2011).

That low-frequency gravity wave generation is connected to the vertical heating structure of an MCS and can cause significant environmental modifications has been well established by previous studies within tropical or mid-latitude daytime environments, yet limited work has addressed gravity wave generation and propagation in more realistic environments common for mid-latitude MCS formation and sustainability. Can N1 gravity wave generation be connected to the cellularity of MCS updrafts? How do low-frequency gravity waves modify the downstream environment, and are these modifications enough to make conditions more or less favorable for cloud development and CI? This study will address these questions as well as their sensitivities to deep vertical wind shear and nocturnal environments to better represent the potential processes occurring in MCSs across the plains through CM1 simulations.

This paper is organized as follows: The methodology and CM1 model configuration can be found in Chapter 2. Chapter 3 sets the foundation for this work through analysis of a highly idealized MCS. Low-frequency gravity wave sensitivities to varying vertical wind and thermodynamic profiles are explored in Chapter 4. Finally, the conclusions from this work will be discussed in Chapter 5.

CHAPTER 2

MODEL CONFIGURATION AND INITIALIZATION

This study employs CM1 (Bryan and Fritsch 2002) to analyze low-frequency gravity waves under non-linear influences involved in MCSs, vertical wind shear, and nocturnal environments. CM1 is a three-dimensional, non-hydrostatic model commonly used to study convection (e.g. Schumacher 2009; French and Parker 2010; Schumacher 2015). The governing equations for the velocity components (u, v, w), nondimensional pressure, potential temperature, and the mixing ratios of water vapor, liquid water (cloud water and rain), and solid water (snow, ice, and hail) are integrated over high temporal and spatial resolutions to simulate idealized atmospheric phenomena. A detailed account of the model configuration can be found in Adams-Selin (2019). The domain extends 350 km in the x direction and 300 km in the y direction, both with 250-m horizontal grid-spacing. The uniform vertical grid-spacing is 100 m through 16 km, all calculated under a 1.5 s time step. Rayleigh damping begins above 14 km where the inverse e-folding time is 1/300 s^{-1}. The "cold pool-dam break" (Weisman et al. 1997) mechanism is used to initiate convection, and the Morrison microphysical parameterization with hail as the dense rimed ice class (Morrison et al. 2009) is utilized to best represent the hydrometeor composition within each MCS to accurately measure the associated latent heating processes. For each input profile, N was smoothed if at any point it was discontinuous or negative to remove unforeseen trapping layers, and the potential temperature was adjusted accordingly assuming no changes to water vapor content.

The first simulation will serve as a base comparison for the following three more realistic simulations. The initial conditions for this control simulation are defined by the Weisman and Klemp (1982) thermodynamic profile, modified to increase the surface mixing ratio to 16.2 g kg^{-1}, paired with a linear vertical wind shear profile of 5 m s^{-1} easterly winds at the surface tapering to 0 m s^{-1} by 5 km. Fovell (2002) and Fovell et al. (2006) used the same vertical wind shear profile as tropical MCSs tend to initiate and propagate in environments with minimal shear in the upper levels accompanied by more pronounced shear below (Fovell 2002).

The next three simulations each incorporate aspects of a sounding collected during PECAN at 0523 UTC 15 July 2015 in Hays, KS. The radiosonde was released just minutes before a particularly active bowing portion of the MCS reached the area. The wind profile is smoothed using the 1-2-1 method, and for the simulations that incorporate this shear profile, a 5.4 m s^{-1} southerly wind was added to the

initialization profile to contain the convection. The thermodynamic profile from this sounding is modified to include an increase in relative humidity by 20% in the lowest 200 mb, the amount of additional moisture needed to produce a MCS similar to the one observed. Increasing the moisture of the initialization environment in order to simulate realistic convection is a common practice (e.g. Peters and Schumacher 2016), and this is particularly true for environments with CIN (Naylor and Gilmore 2012), as in this sounding. Although the additional moisture increases the most unstable convective available potential energy (MUCAPE) from 5320 J kg^{-1} to 8164 J kg^{-1}, the MCSs initialized using this thermodynamic profile share a similar intensity to the observed PECAN MCS as detailed in Chapter 4.3. The temperature and relative humidity profiles are also smoothed by the 1-2-1 method, and stratospheric variables were extrapolated from approximately 14 km to 16 km.

To understand the sensitivity of low-frequency gravity waves to vertical wind shear more common of mid-latitude MCSs, the second CM1 simulation of this study uses the same thermodynamic profile as the control simulation but incorporates the smoothed vertical wind profile collected from the PECAN sounding for the initial conditions. The next experiment serves to isolate how a nocturnal thermodynamic environment may modify gravity wave generation, propagation, and influence independent of the wind profile. The sounding used to initialize this simulation utilizes the same idealized wind shear profile as the control simulation but includes the modified version of the thermodynamic profile from the PECAN sounding. Finally, the last simulation acts to represent every aspect of a nocturnal MCS including a low level jet (LLJ) as well as a stable boundary layer. This simulation was initialized using the modified wind and thermodynamic profiles of the PECAN sounding.

CHAPTER 3

ANALYSIS OF AN IDEALIZED MCS

3.1 STRUCTURE

A highly idealized MCS simulated in CM1 is used in this analysis to provide a foundation for low-frequency gravity wave generation and propagation in which the sensitivities of these to changes in the initial thermodynamic and vertical wind profiles will be discussed. The sounding used to initialize this control simulation, as seen in Fig. 3.1, includes 5 m s^{-1} of easterly shear at the surface linearly decreasing to 0 m s^{-1} by 5 km and a slightly modified Weisman and Klemp (1982) thermodynamic profile smoothed to remove any trapping layers. This environment produced an organized MCS with an expansive trailing stratiform region as seen in the horizontal cross section of surface reflectivity in Fig. 3.2 (a).

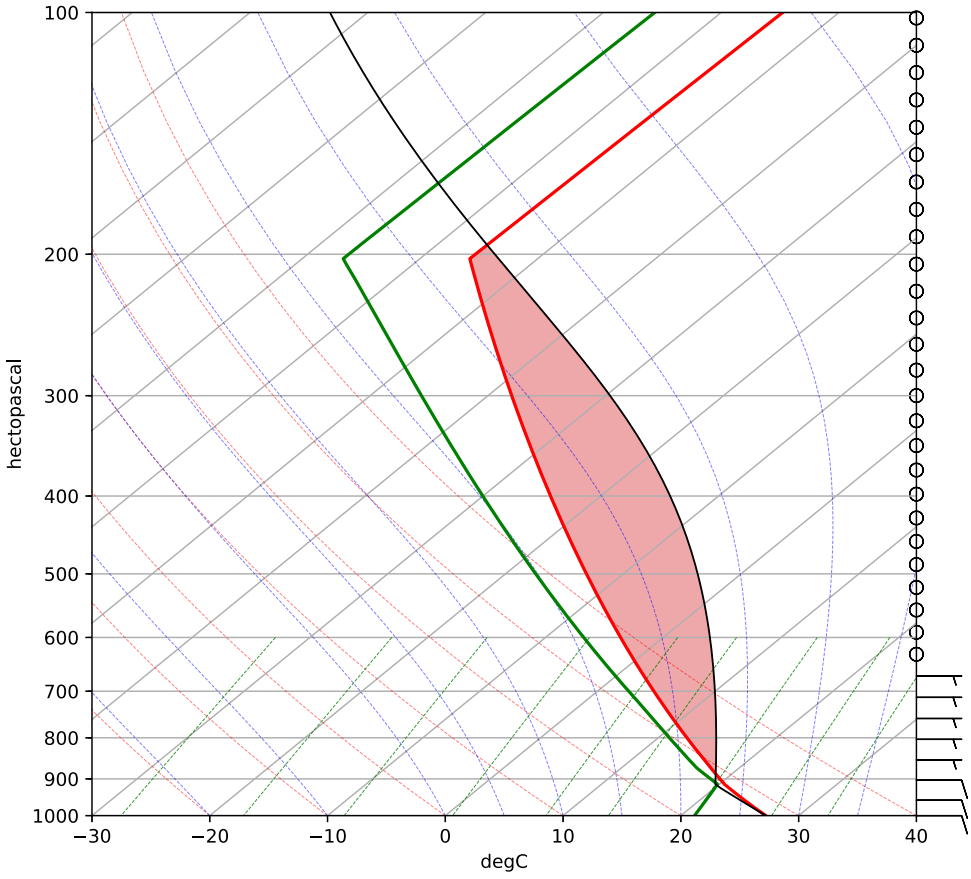

FIG. 3.1. Skew-T Log-P diagram of the sounding used to initialize the control simulation. The black line delineates the parcel path, and the red shaded region indicates CAPE in J kg^{-1}.

The first reflectivity values appear approximately 14 minutes into the simulation at heights of 4-5 km, indicating the initiation of the storm and the presence of an updraft. Eight minutes later, precipitation descends upon the surface. "Fingers" of reflectivity often protrude from the convection parallel to the vertical wind shear vector, an element previously examined within idealized models by Bryan et al. (2007) but also noted as a feature observed in many of the MCSs studied in the PECAN field campaign (Geerts et al. 2017). Other than these convective rolls, this simulation did not have any CI or cloud development downstream.

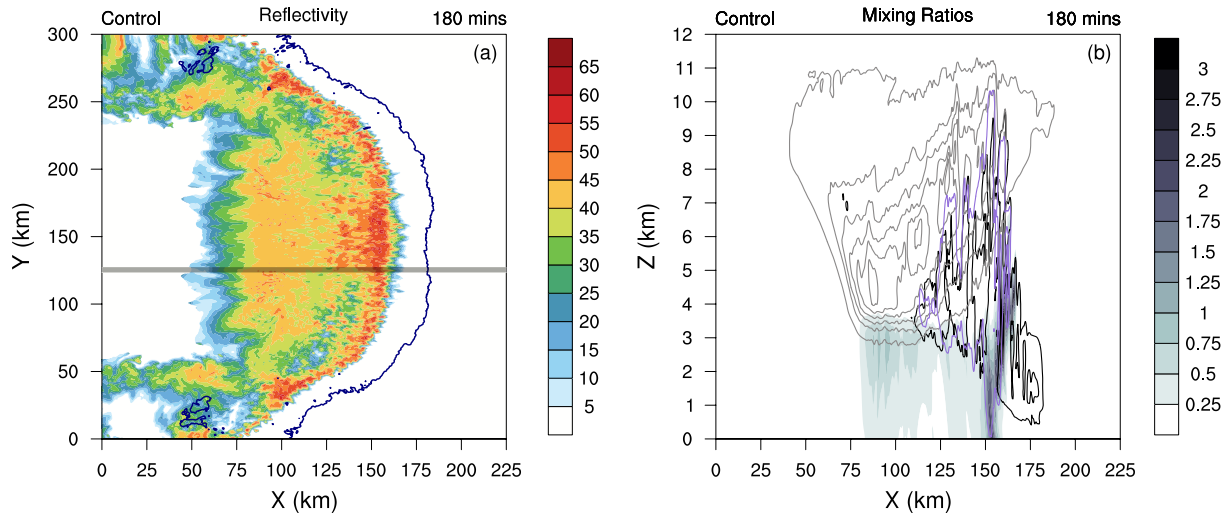

FIG. 3.2. (a) Horizontal cross section of surface reflectivity at t = 180 minutes. The navy contour delineates the cold pool, and the gray line at y = 125 km represents the 5 km cross section for which all analysis was averaged over. Mixing ratios of the hydrometeors comprising the MCS, calculated over the y cross section in (a) for the same time, are shown by the vertical cross section in (b) in g kg^{-1}. The gray contours represent combined snow and ice mixing ratios (q_i) from 0.2 to 4.4 by 0.06, purple contours are hail (q_h) from 0.1 to 4.1 by 1, black contours are cloud water (q_c) from 0.1 to 3.1 by 1, and the filled color contours show the rain mixing ratios (q_r).

Mixing ratios of various hydrometeors shown in Fig. 3.2 (b) demonstrate the internal dynamics and immediate environmental influence of the MCS. Periodically lofted hail within the convective region reveals a cyclical nature in the updrafts of the MCS, shown in Fig. 3.3, speaking to the modest strength of the system. Due to the lack of wind shear in the mid to upper levels, the presence of hail does not extend far behind the convective updrafts, leaving the stratiform region to be primarily composed of cloud ice and rain. Considering the overall absence of hail and relatively small mixing ratio values of other hydrometeors within the stratiform region, the highest rates of latent cooling occur within the convective downdrafts (a feature also noted in McAnelly et al. 1997), although latent cooling is present throughout the expanse of the stratiform region as well (not shown).

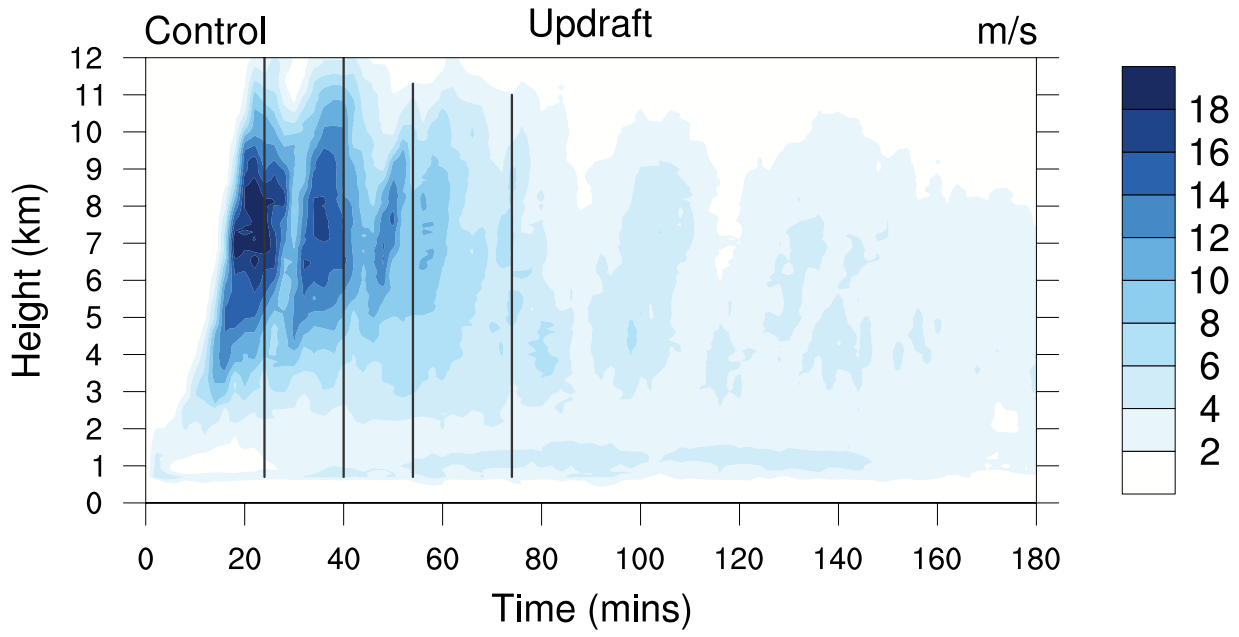

FIG. 3.3. Time-height diagram of the 95^{th} percentile values of updraft velocity in m s^{-1}. The vertical gray lines indicate approximate times of N1 gravity wave generation as determined from Fig. 3.5.

3.2 N1 GRAVITY WAVE GENERATION

The onset of the updraft releases a large amount of latent heat due to the rapid development of hydrometeors. The additional heat provides buoyancy within the convection which acts to reinforce the updraft, and the process repeats. The rate of latent heat release as well as the updraft velocity both demonstrate a cyclical nature with lifecycles between 15-20 minutes as shown in Figs. 3.4 and 3.3 respectively. Lane and Zhang (2011) connected the frequency of deep-tropospheric gravity waves observed in cloud fields to the frequency of convective surges, implying a relationship between gravity wave generation with the initiation of new single cells and their associated updrafts and latent heat release. Applying this understanding to the updrafts within MCSs, Adams-Selin and Johnson (2013) and Adams-Selin (2019) found that in many instances, a N1 gravity wave was generated in step with fluctuations in the updraft. The cyclical nature of the updraft and latent heat release within this simulation implies that there should be a number of N1 gravity waves generated from this system in response to changes in the vertical latent heating profile.

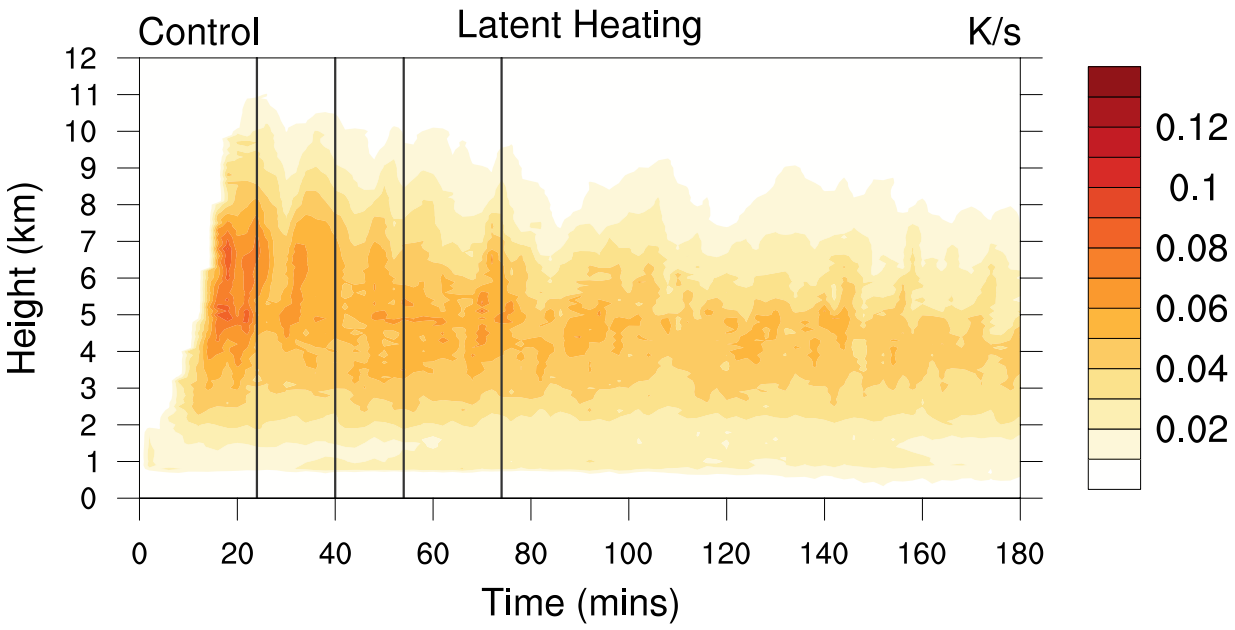

FIG. 3.4. Time-height diagram of the 95^{th} percentile values of positive changes to the potential temperature field due to microphysical processes in K s^{-1}. The gray lines indicate approximate times of N1 gravity wave generation as determined from Fig. 3.5.

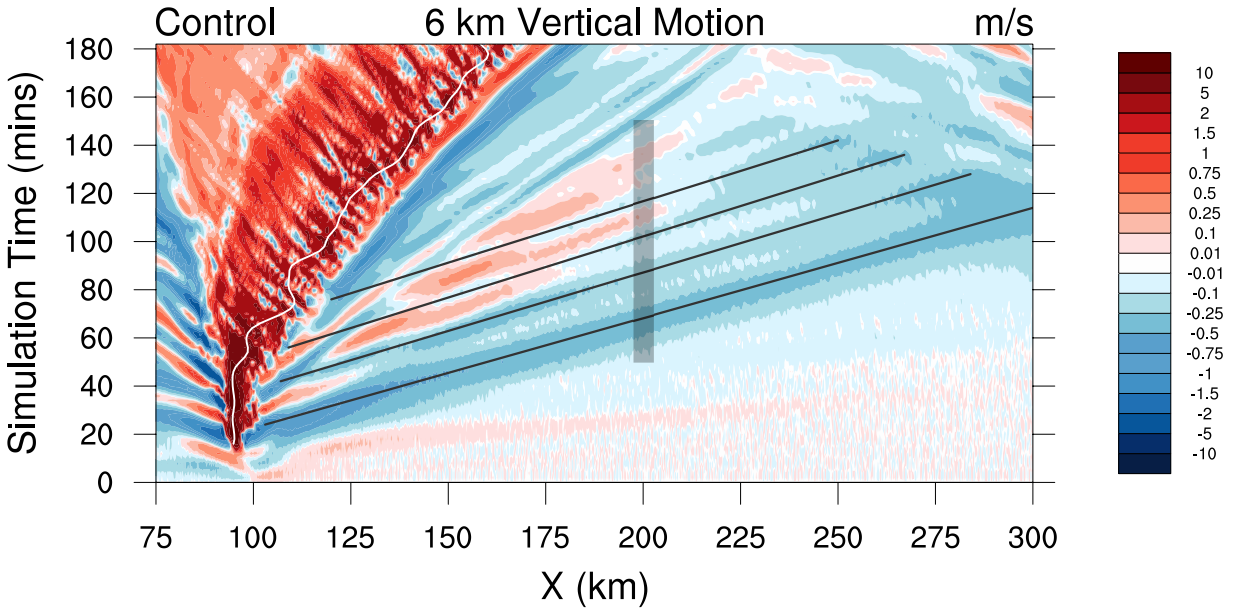

FIG. 3.5. Hovmöller diagram of vertical motion at 6 km in m s^{-1}. Gray lines delineate each N1 gravity waves' propagation downstream. The white line is the location of the maximum updraft velocity at this height, and the transparent black box centered over x = 200 km shows the domain of pre-convective descent analyzed in spectral analysis.

The first N1 gravity wave appears approximately 20 minutes into the simulation as the storm begins to develop and the updraft takes form. Cycling of the updrafts generates more N1 waves in response, and these appear after each respective maximum in latent heat release shown by the gray lines in Fig. 3.4. As the storm matures, the updrafts and associated latent heat release weaken in intensity with each cycle, consequentially generating weaker N1 gravity waves (shown by the decrease in magnitude of descent with each wave path in Fig. 3.5). These waves are moving at approximately 35.2 m s^{-1} after removing the mean tropospheric zonal wind of -1.09 m s^{-1}, which matches well with the theoretical speed of 38.2 m s^{-1} calculated from Eq. (1.1) for an average column N of 0.01 s^{-1} and a tropopause height of 12 km, both derived from the start of the simulation.

3.2.1 Spectral Analysis

As the storm matures and begins to develop a trailing stratiform region, gravity waves become increasingly difficult to subjectively discern after extensive environmental modulation by preceding wave activity closer to the convective line. To objectively identify the frequency of N1 initiation and subsequent influence on the forward environment, spectral analysis is performed on three principal variables within this mechanism: the updraft and latent heat release as signals for generation, and deep-tropospheric descent as the downstream influence. A time-series of the 95^{th} percentile values of updraft velocity and latent heat release between 5 to 8 km are represented by the gray and red lines respectively in Fig. 3.6. While their values are maximized at initiation of the MCS, there is a clear cyclical nature in both the updraft speed as well as the latent heating, and they vary concurrently. The 95^{th} percentile values of deep tropospheric descent in the domain ahead of the convective line (shown by the black box in Fig. 3.5) between the same heights is indicated by the blue line. For all negative variables within this thesis, the 95^{th} percentile corresponds to magnitude. As waves begin to travel across the analysis domain centered at x = 200 km starting around 60 minutes, the time-series of descent shows periodicity similar to the cyclical nature of the updraft and latent heating time-series.

Spectral analysis is employed to distinguish sine and cosine wave patterns within these time series to objectively identify at what frequency they each demonstrate cellularity. After removing the series mean and least squares linear trend, each time period of analysis is tapered by 10% to avoid spectral leakage. This statistical method is first applied to the updraft and latent heating time series between 10-110 minutes. To increase the degrees of freedom, the power spectrum is calculated every 250 m for 5 km centered about y = 125 km, the domain which this analysis usually averages over. At this spatial resolution, the power spectrum is then calculated for 21 time-series. General model output is able

to resolve independent features approximately every 6-10 Δx (Skamarock 2004), therefore this study will approximate 6 degrees of freedom for the spectra. The same process was conducted for the pre-convective descent time series between 50-150 minutes.

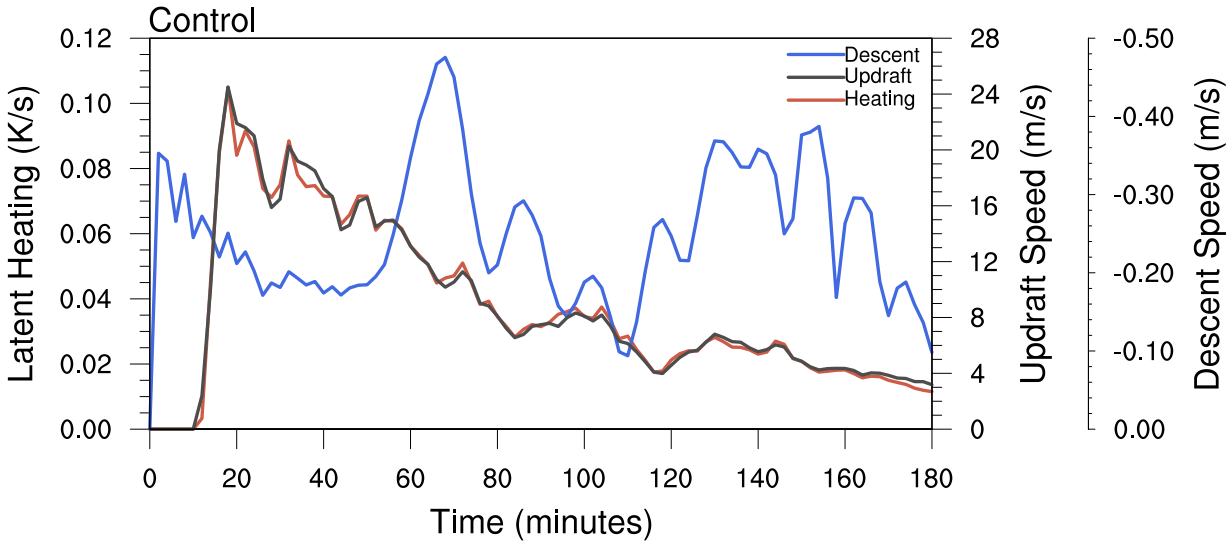

FIG. 3.6. Time-series of the 95^{th} percentile values of the updraft velocity, microphysical heating, and pre-convective descent represented by the gray, red, and blue lines respectively. The area over which the pre-convective descent is calculated is shown in Fig. 3.5.

The power spectrum for updraft velocity, latent heat release rates, and pre-convective descent can be seen in Fig. 3.7. The solid lines define the spectra for each variable, and the respective dashed lines represent the 90% confidence interval against a red noise null hypothesis, defined as being significant in this study. At 0.12 cycles/2 minutes (the model output frequency), each variable has a significant peak, indicating that these three parameters show maximums at the same frequency. This frequency corresponds to an N1 gravity wave being generated and having a significant environmental influence downstream around every 17 minutes, which matches with the frequency of gravity wave generation subjectively identified in the 6 km vertical motion Hovmöller diagram in Fig. 3.5 as well as the time-height diagrams of updraft velocity and latent heat release seen in Figs. 3.3 and 3.4. This strongly suggests that the N1 waves are generated by alterations in latent heating due to the cyclical variations in the updrafts, and the same N1 waves lead to regular perturbations of mid-level descent up to 100 km ahead of the system. These robust results suggest that even as the stratiform region expands and becomes increasingly more influential on the MCS latent heating profile as shown in Fig. 1.1 (b) and discussed in

Houze (2004), N1 waves are likely still being generated through 110 minutes into the simulation alongside higher order wave modes even though their influence may become harder to subjectively discern downstream.

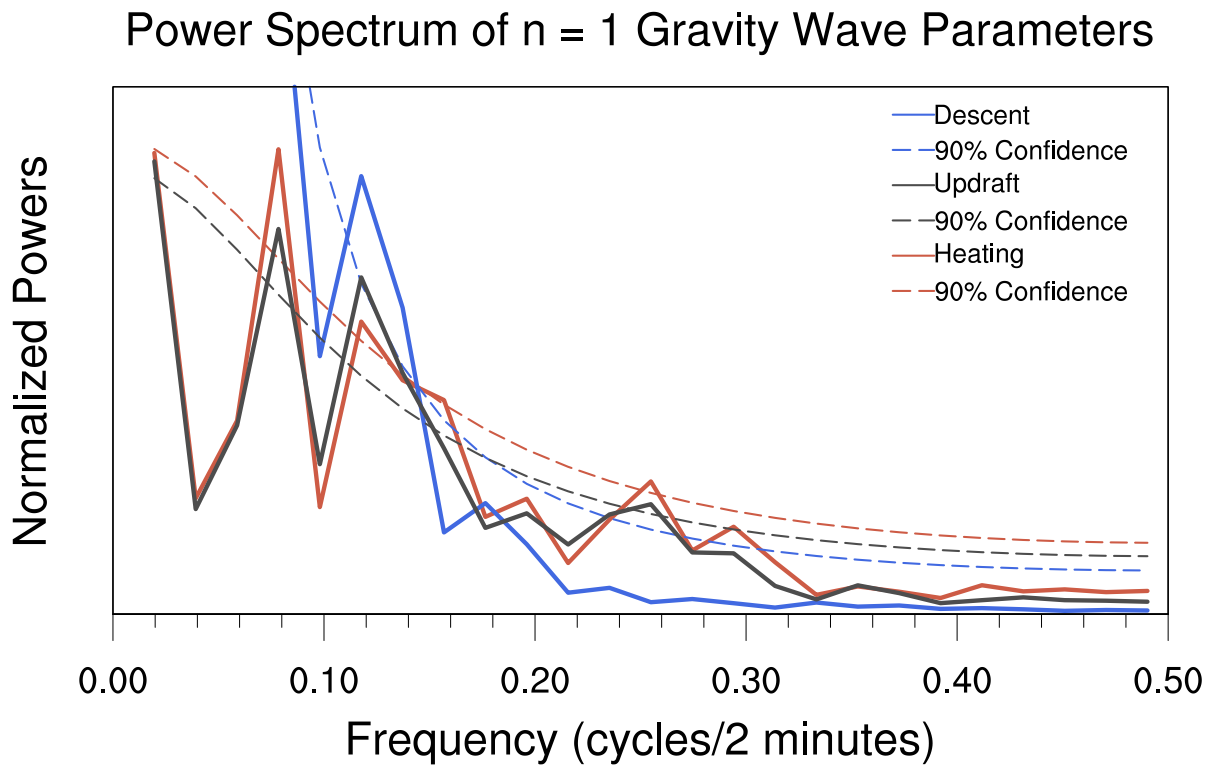

FIG. 3.7. The power spectrum for updraft velocity (gray), latent heat release rate (red), and pre-convective descent (blue). Dashed lines represent the 90% confidence intervals for each variable of the same color. Each spectra was normalized so that the area under the line equals the variance of the detrended time-series.

3.3 N2 GRAVITY WAVE GENERATION

As the MCS transitions into maturity, the convective updrafts lower in height and weaken in intensity, the latent heating is reduced, and another mode of low-frequency gravity waves becomes more favorable for generation (Lane and Reeder 2001). N2 waves, which travel at about half the speed of their N1 counterparts at a theoretical speed of approximately 20 m s^{-1} for this environment, are generated in response to increases in cooling within the lower half of the troposphere associated with sublimation, melting, and evaporation of hydrometeors largely below the freezing level and cloud base. A time-height diagram of the changes in the potential temperature field due to these latent cooling processes can be seen in Fig. 3.8 which exhibits a clearly defined melting level around 4 km.

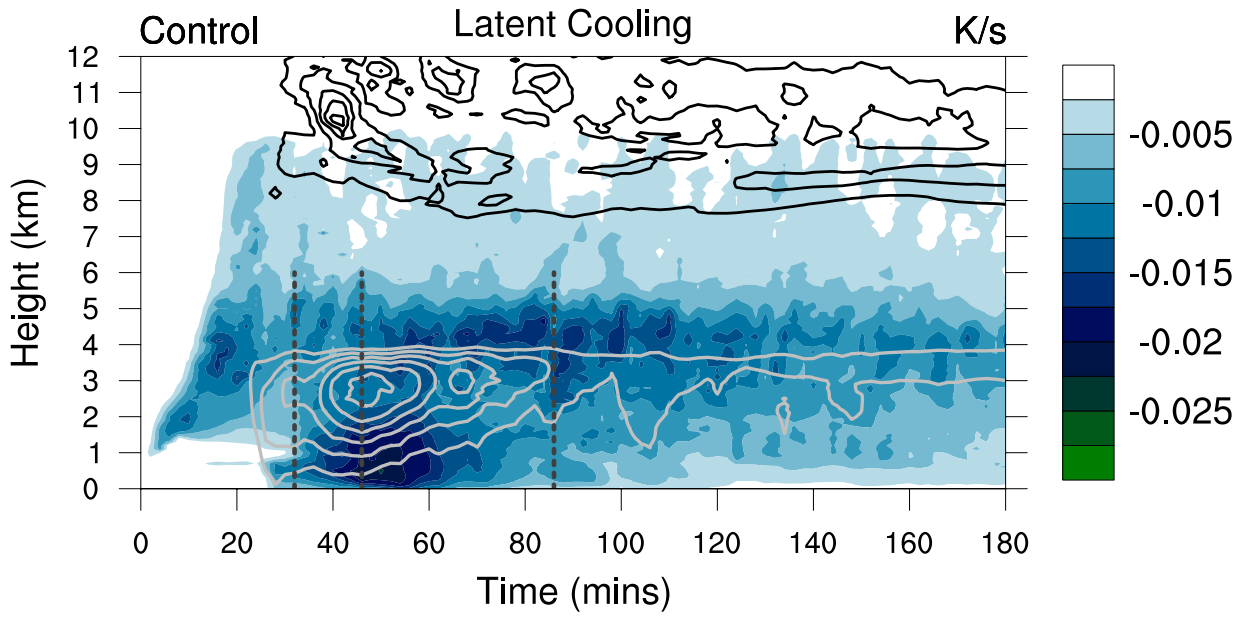

FIG. 3.8. Time-height diagram of the 95^{th} percentile values of negative changes to the potential temperature field by microphysical processes in K s^{-1}. Shaded colors show rates of evaporational cooling. Latent cooling due to melting is represented by the light gray contours from -0.14 to -0.002 by 0.002, and the black contours show cooling from sublimation from -0.75 to -0.05 by 0.1. Dashed gray lines indicate approximate times of N2 gravity wave generation as determined from Fig. 3.9.

While the N1 generation mechanism and timing are more uniform, the same can not be said for N2 waves. Owing particularly to the fact that stratiform precipitation and mesoscale downdrafts determine magnitudes of latent cooling within an MCS, and by extension N2 gravity wave generation, their dynamics are much less cyclical and can be more sporadic in nature. The first distinguishable N2 gravity wave is generated roughly 30 minutes into the simulation with the onset of latent cooling as rain and hail descend to the surface. The second wave, generated approximately 45 minutes into the simulation, occurs in response to a surge of cooling as the storm begins to widen and separate into two distinct regions of stratiform and convective precipitation, a generation mechanism also noted in Fovell (2002) as the MCS transitioned into maturity. As shown by the second dashed line in Fig. 3.8, this generates the largest latent cooling response, with the highest values of melting and evaporation seen in the entire simulation occurring at this time. As a result, the consequent N2 wave has the largest associated low-level ascent, and its downstream impact can be seen by the second dashed line in Fig. 3.9. The third subjectively analyzed N2 gravity wave is the hardest to distinguish with only a small increase in latent cooling due to melting observed around the time of generation (approximately 85 minutes).

Likely the most important factor in the generation of this wave was the overall weakening of the MCS that begins around this time. Although there is not a large change to the rates of latent cooling, the subsiding latent heat release changes the vertical potential temperature profile within the MCS to be more neutral in the upper levels, and in combination with the cooling dominance in the lower levels, strongly aids in the generation of this wave.

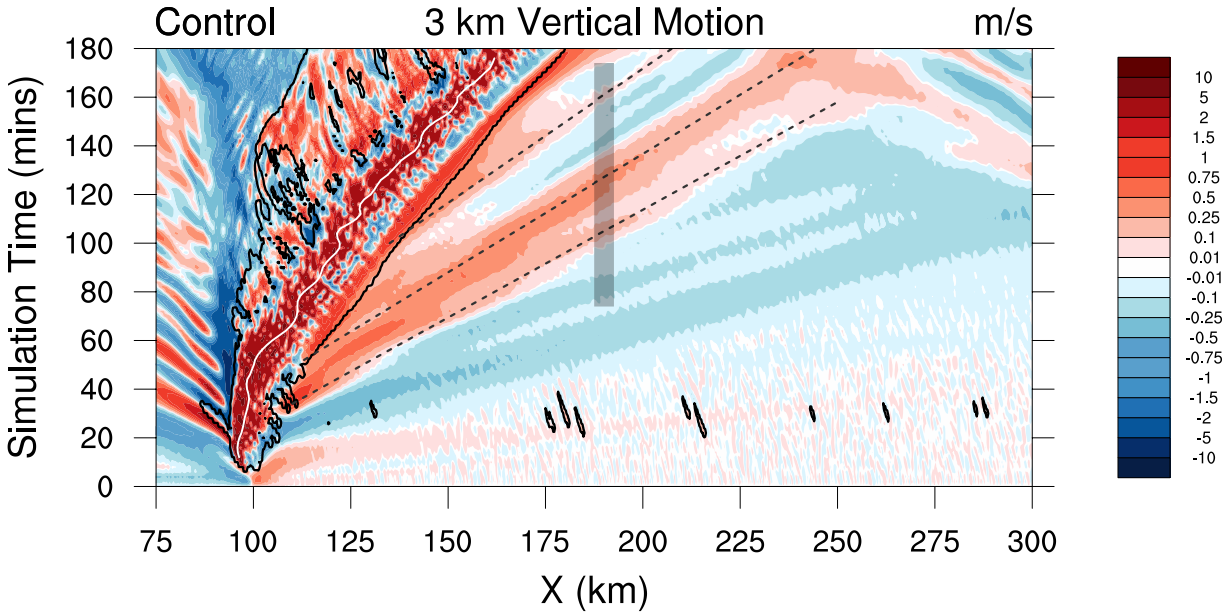

FIG. 3.9. As in Fig. 3.5 but at z = 3 km. Dashed gray lines show three N2 waves and their propagation ahead of the convective line. The transparent black box centered over x = 190 km shows the domain of pre-convective ascent analyzed in spectral analysis

3.3.1 Spectral Analysis

Owing to N2 waves being harder to subjectively identify, spectral analysis is performed as a method of identification but also in attempt to find a pattern among them. If there is a clear cyclical signal among the generation mechanisms as well as subsequent upward motion downstream, the frequencies of perturbations in the downdraft velocity, latent cooling rates, and ascent ahead of the convective line should relatively match just as they did for the N1 waves. A time-series of the 95^{th} percentile values of downdraft speed and latent cooling rates between 1 to 4 km are represented by the black and teal lines respectively in Fig. 3.10. The 95^{th} percentile values of ascent between the same heights in the domain ahead of the convective line (shown by the black box in Fig. 3.9) are indicated by the purple line. The analysis was performed with the same specifications as for the N1 waves, but the downdraft and latent cooling rates were analyzed between 16 and 116 minutes, and the pre-convective ascent was analyzed

between 74 and 174 minutes due to the slower propagation speed of N2 waves. Results indicate that there is no matching spectra between the three variables as seen in Fig. 3.11. Since these processes are much less cyclical, the analysis cannot as easily identify waves within their time series. However, this is not particularly surprising. N2 wave generation mechanisms are not nearly as cyclical in nature as those of the N1 waves, and the surges in latent cooling as seen in Fig. 3.8 do not show a regular pattern. The downdraft and latent cooling do not always vary concurrently with time although the majority of cooling is restricted to the convective region, and spectral analysis helps to show that the they act more chaotically compared to the updraft and latent heat release.

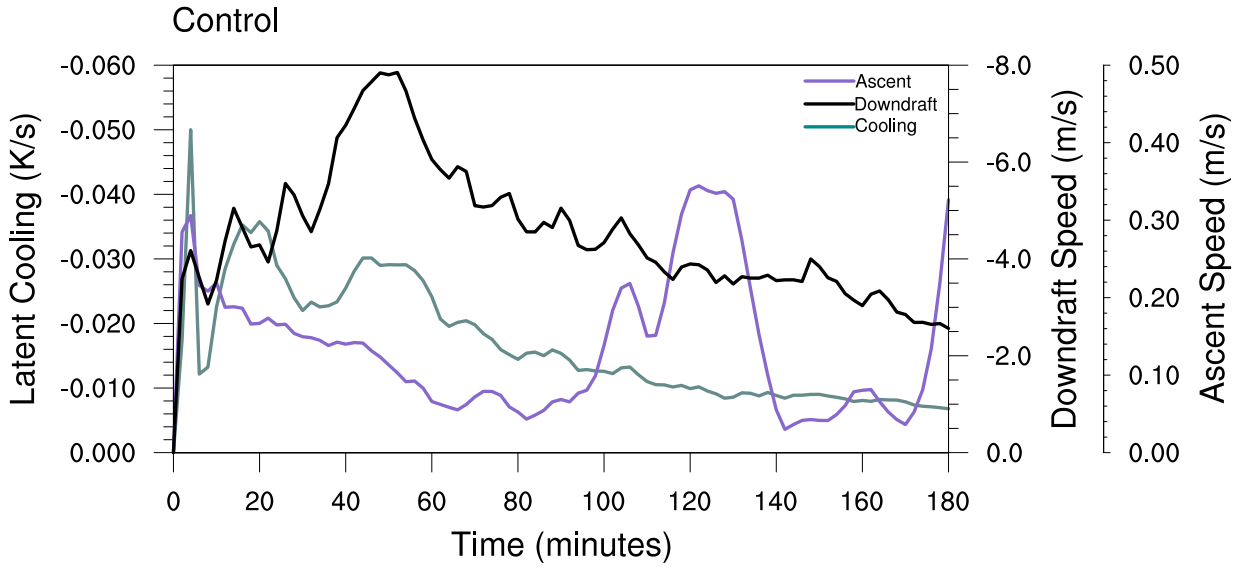

FIG. 3.10. As in Fig. 3.6 but for the 95^{th} percentile values of the downdraft speed (black), latent cooling (teal), and pre-convective ascent (purple). The area over which the ascent is calculated is shown in Fig. 3.9.

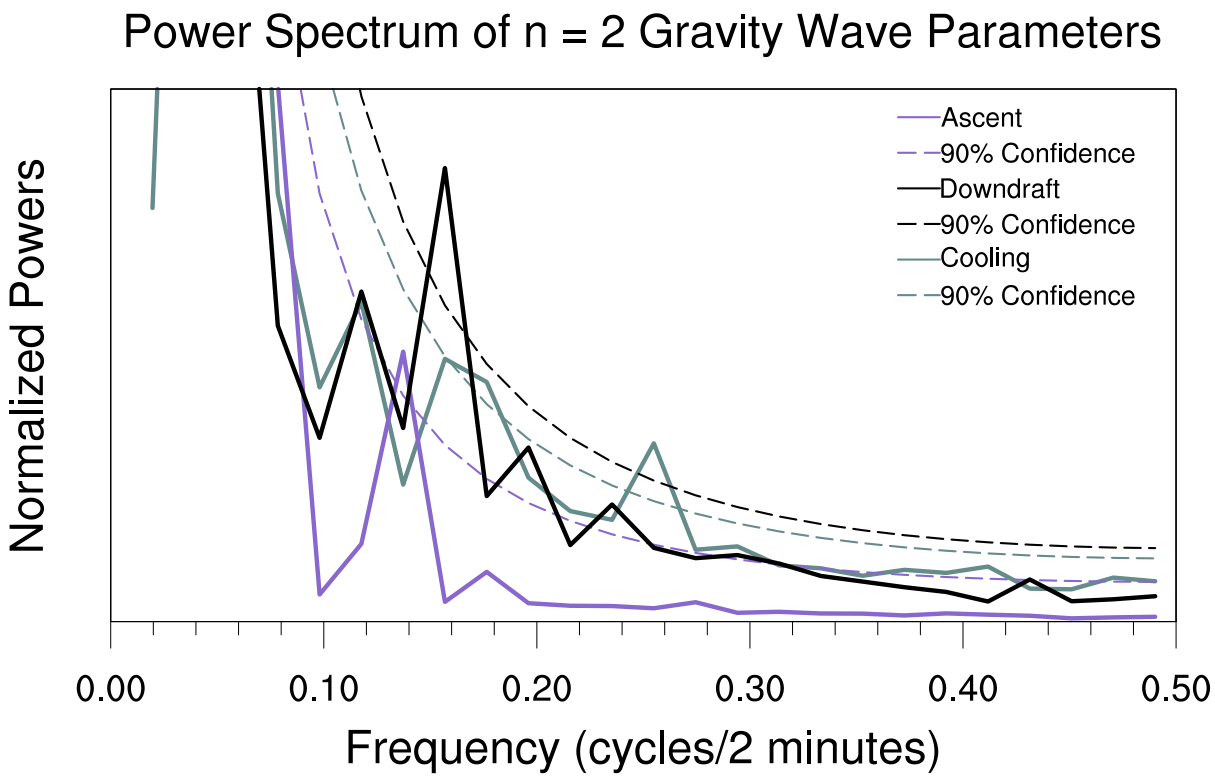

FIG. 3.11. As in Fig. 3.7 but for the power spectrum of downdraft speed (black), latent cooling (teal), and pre-convective ascent (purple).

3.4 ENVIRONMENTAL RESPONSE

Although the control simulation does not demonstrate CI or discrete propagation, the waves still have a notable impact downstream of the MCS. As discussed above and in Nicholls et al. (1991), N1 waves manifest themselves through deep-tropospheric descent ahead of the convective updrafts, maximizing around half the height of the tropopause, or 6 km in this simulation. By looking at a Hovmöller diagram of vertical motion at that height, N1 waves can be tracked as they move through the forward environment. Four such waves are analyzed and shown by the solid gray lines in Fig. 3.5, where each wave has decreasing magnitudes of descent due to the respective reduction in rates of latent heating with time as shown in Fig. 3.4. Additionally, N2 waves can be identified in the same manner by ascent through the lower half of the troposphere. Considering that latent cooling within this simulation reaches peak intensity around 3 km as seen in Fig. 3.8, N2 waves in this simulation can be tracked as they propagate downstream by following areas of enhanced ascent at 3 km in Fig 3.9.

Each wave mode has a particular area of influence that can potentially act to suppress or support the stability of the downstream environment. The first two N1 waves adiabatically warm the depth of

the troposphere through descent, reducing the MUCAPE field by over 100 J kg^{-1} for each wave passage as shown by the solid lines in Fig. 3.12. The greatest heating occurs where the descent is strongest, in the mid-levels, and so the influence on CAPE from N1 waves is particularly strong. The ascent corresponding to N2 waves helps to partially recover the MUCAPE field with each wave passage by moistening and cooling the lower levels. However, the peak influence of this cooling is co-located with the peak in ascent, which occurs around 3 km in this environment. This causes N2 waves to have less of an influence on the CAPE field, but a greater and more expansive influence on the LFC. As seen in Fig. 3.13, the deep-tropospheric descent and adiabatic warming induced by the two N1 waves causes the LFC to increase by at least 25 meters. However, the N2 waves work to counteract the influence of the N1 waves by lowering the LFC, where the first N2 wave, generated by the onset of precipitation to the surface, lowers the LFC by 25 meters, and the second, stronger N2 wave acts to lower the LFC even past its original height. These results are consistent with those found in Lane and Reeder (2001), Adams-Selin and Johnson (2013), and Adams-Selin (2019), who agree that each wave's height of maximum influence highlights changes in different stability parameters.

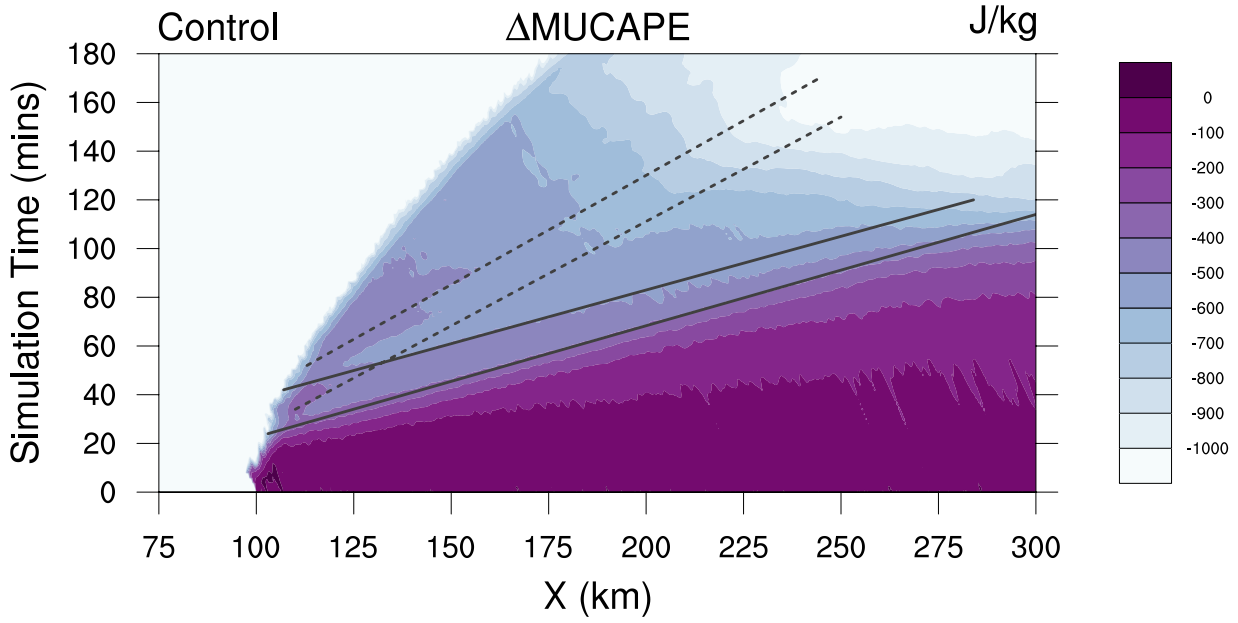

FIG. 3.12. Hovmöller diagram of the change in MUCAPE from the initial environment (J kg^{-1}). The solid lines show the paths of the first two N1 waves and the dashed lines the first two N2 waves.

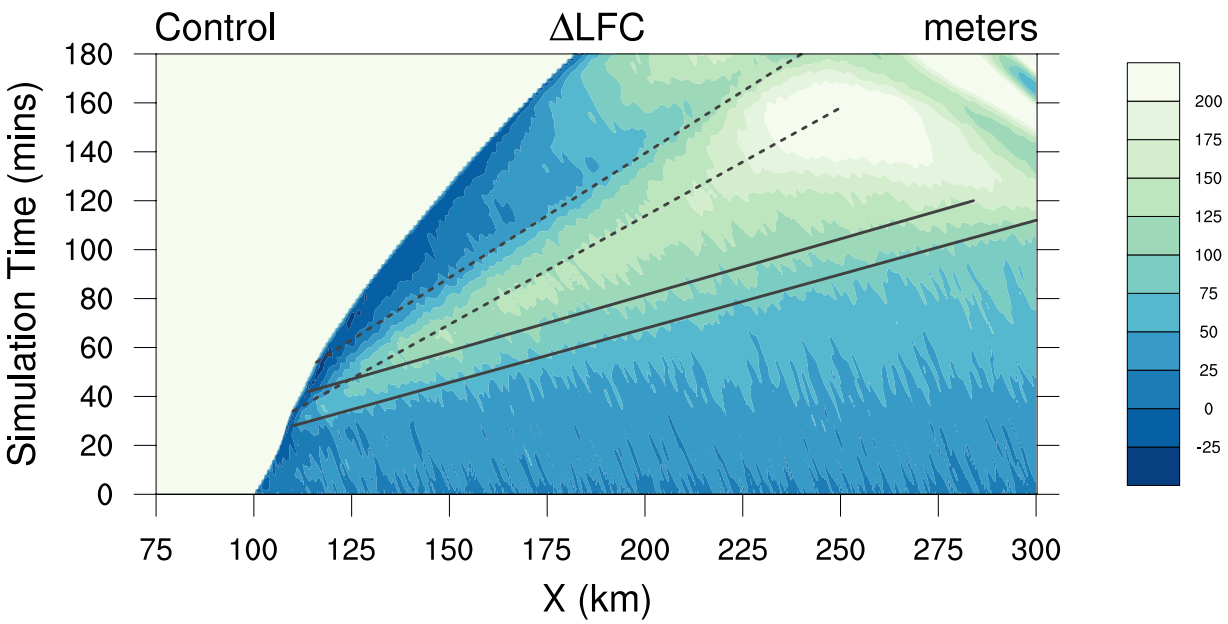

FIG. 3.13. As in Fig. 3.12 but for the LFC in meters.

CHAPTER 4

MCS AND LOW-FREQUENCY GRAVITY WAVE SENSITIVITIES

This work has established that low-frequency gravity wave generation, strength, and propagation are dependent upon the internal processes of a MCS. These results, however, were articulated for a highly idealized environment. The rest of this thesis will focus on a series of sensitivity tests in which low-frequency gravity waves are studied within more realistic environments and accordingly constructed by more realistic MCSs. To understand the sensitivity of these waves to deep vertical wind shear, a second CM1 simulation, hereafter defined as the Wind simulation, is run that maintains the idealized Weisman and Klemp (1982) thermodynamic environment but includes the vertical wind profile from the 15 July 2015 Hays, KS sounding mentioned in Chapter 2. The next experiment uses the modified thermodynamic profile from the Hays, KS sounding with the idealized linear shear profile of the control run to isolate the response of low-frequency gravity waves to a nocturnal environment and will further be referred to as the Thermo simulation. The final simulation created for this thesis, hereafter the Nocturnal simulation, acts to culminate the findings from the previous three simulations and apply those results and sensitivities to a true nocturnal MCS.

4.1 VERTICAL WIND SHEAR

The distinction between the control run and this simulation lies within their vertical wind profiles. The control simulation uses an idealized wind profile common for sustained MCSs (Rotunno et al. 1988), while this simulation utilizes an observed sounding taken during PECAN minutes before an MCS passed over the area. This vertical wind shear profile introduces veering winds from the surface through the mid-levels with the inclusion of a LLJ below moderate westerly shear aloft. Dissimilarities between the simulations are the result of deep shear impacts on the internal dynamics of a MCS and resultant gravity wave generation. The sounding used to initialize this simulation can be seen in Fig. 4.1. Unique to this case is that it is the only one to develop spurious convection ahead of the MCS. While this convection is likely a result of model noise, the impacts that gravity waves have on the single convective cells and how they are potentially able to support or suppress them can still be studied.

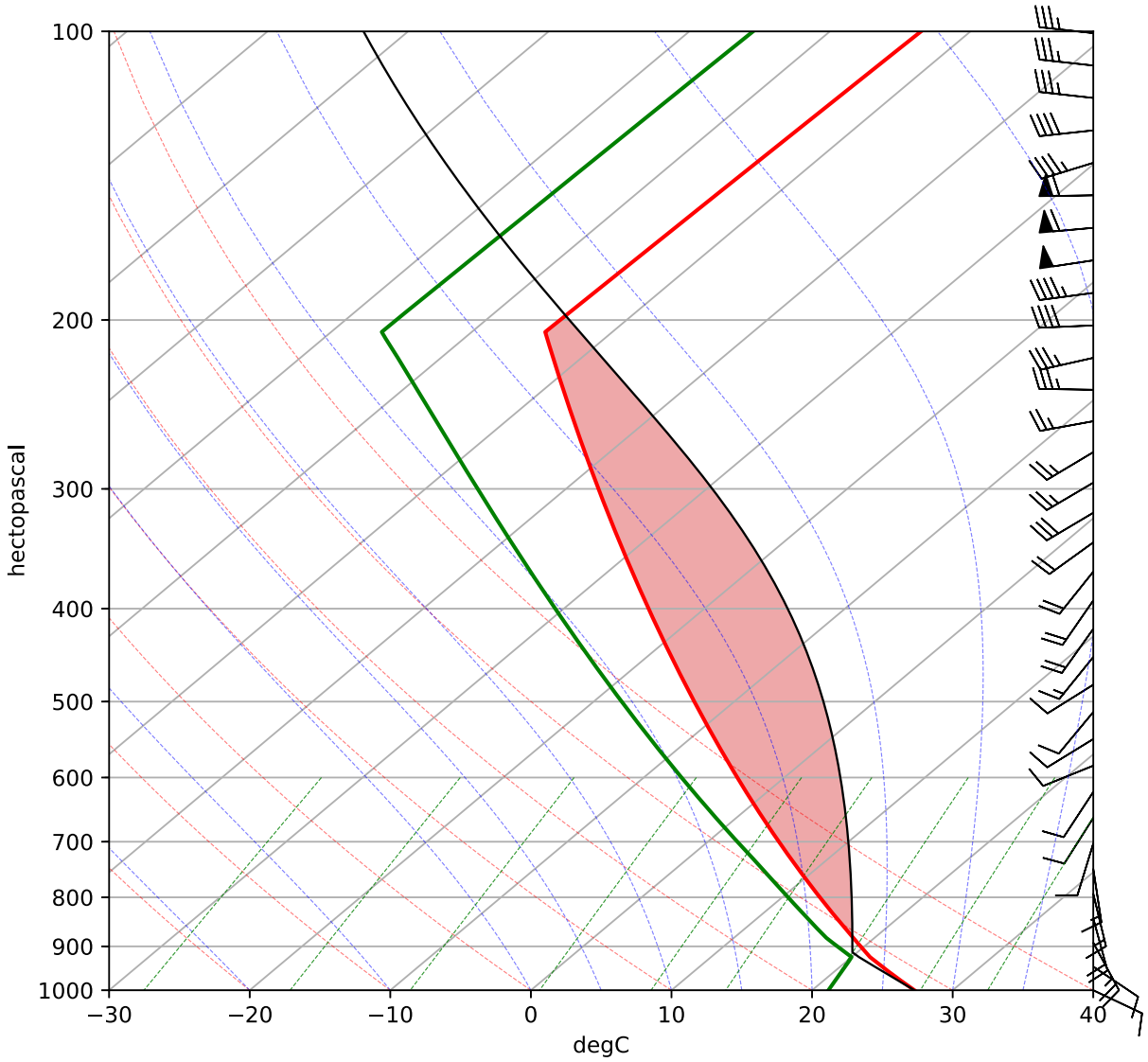

FIG. 4.1. As in Fig. 3.1 but for the input sounding used to initialize the Wind simulation.

Convection first reaches the surface approximately 20 minutes into the simulation in a clear north to south orientation. The MCS exhibits "fingers" of reflectivity extending ahead of the leading line just as in the control simulation, but those quickly diminish around the same time that the spurious convection appears within the domain approximately 50 minutes into the simulation. Bowing of the MCS is apparent after the storm reaches maturity and can be seen in Fig. 4.2 (b). Quickly thereafter, an interesting feature that resembles a wake-low appears on the southern end of the MCS. Also exclusive to this simulation is the strengthening of the MCS with the ingestion of a small convective cell seen approximately 75 km ahead of the convective line in Fig. 4.2 (b). By 150 minutes into the simulation, the storm has weakened considerably and appears to be in its dissipating stages until the additional

moisture and buoyancy from the absorbed cell aids in the revival of the MCS. Immediately following, the updraft velocity and associated latent heat release both show increases in magnitude as seen in Figs. 4.3 and 4.4 (a) respectively. This succession has also been observed in Adams-Selin and Johnson (2013) and Fovell et al. (2006). How the ingested cell was strengthened by an N2 wave as it approached the MCS is discussed in section 4.1.3.

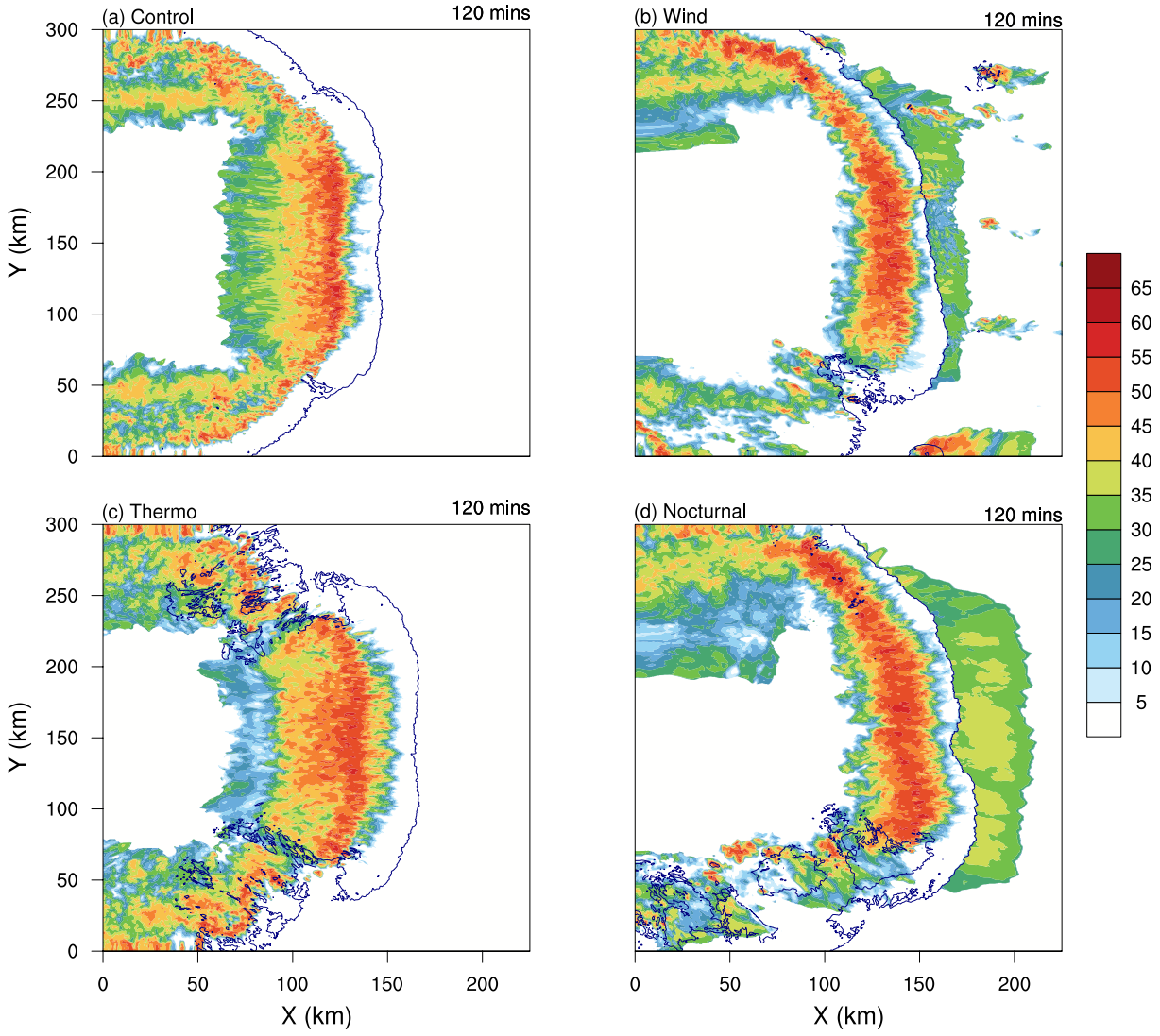

FIG. 4.2. Surface reflectivity at t = 120 minutes for the mature MCSs within the (a) Control, (b) Wind, (c) Thermo, and (d) Nocturnal simulations with their respective cold pools indicated the by navy contours.

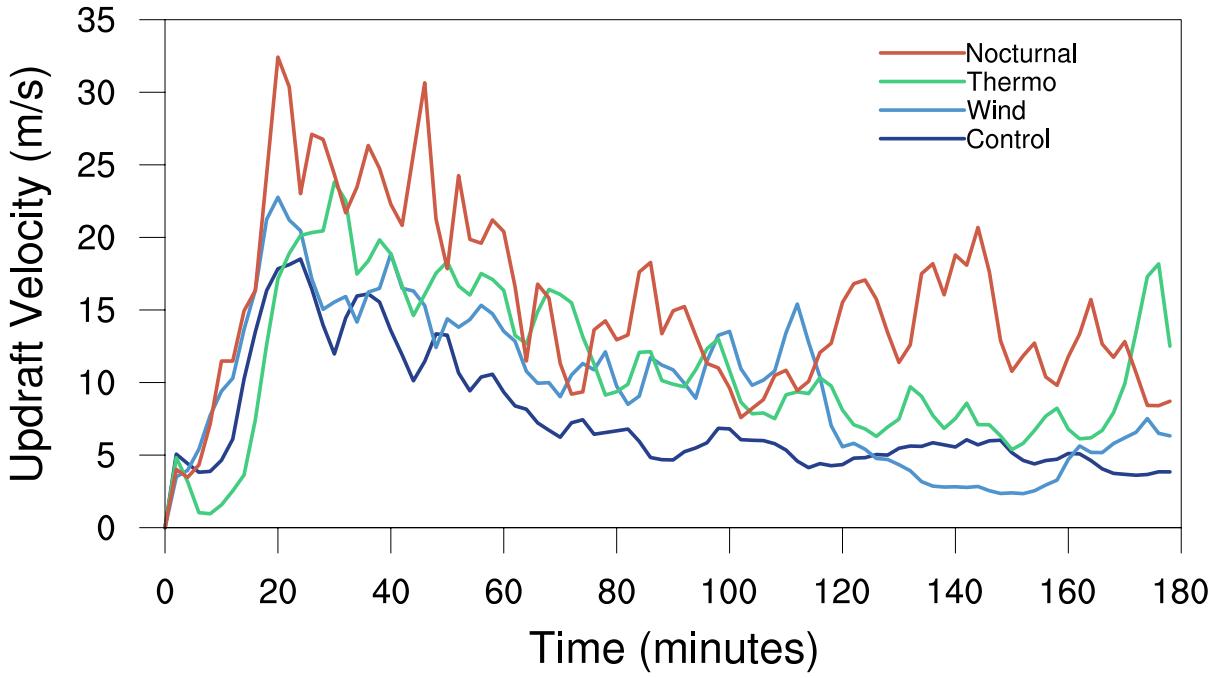

FIG. 4.3. 99^{th} percentile values of vertical motion within the troposphere for the Control (navy), Wind (light blue), Thermo (green), and Nocturnal (red) simulations.

There are a few key differences between the internal dynamics and structure of the MCS in this simulation and the control run that contribute to changes in low-frequency gravity wave generation and strength. From Fig. 4.2, most notable is that the trailing stratiform region for the Wind simulation MCS is much more confined. The horizontal area covered by the convective and stratiform precipitation regions in the control simulation extends almost 125 km at its widest point while the Wind simulation MCS is much smaller in comparison at around 80 km. This drastically restricts the horizontal extent over which latent cooling occurs, placing the vast majority of cooling within the convective downdrafts compared to the moderate distribution of cooling over the stratiform region of the control MCS (not shown). The Wind simulation MCS is also stronger in overall intensity as shown by the higher updraft velocities for this case in Fig. 4.3. Reflectivity values of over 60 dBZ are often lofted high into the storm, sustained for a longer period of time, and occur later into the simulation compared to the control run. However, this MCS also experiences a much more complicated life cycle as it weakens and almost dissipates towards the end of the 3 hour simulation (shown by the rapid decrease in updraft velocity after 115 minutes in Fig. 4.3). The absorbed cell rescues the MCS and helps to re-invigorate the system. All of these factors act to alter the distribution of the latent heating field critical for gravity wave generation.

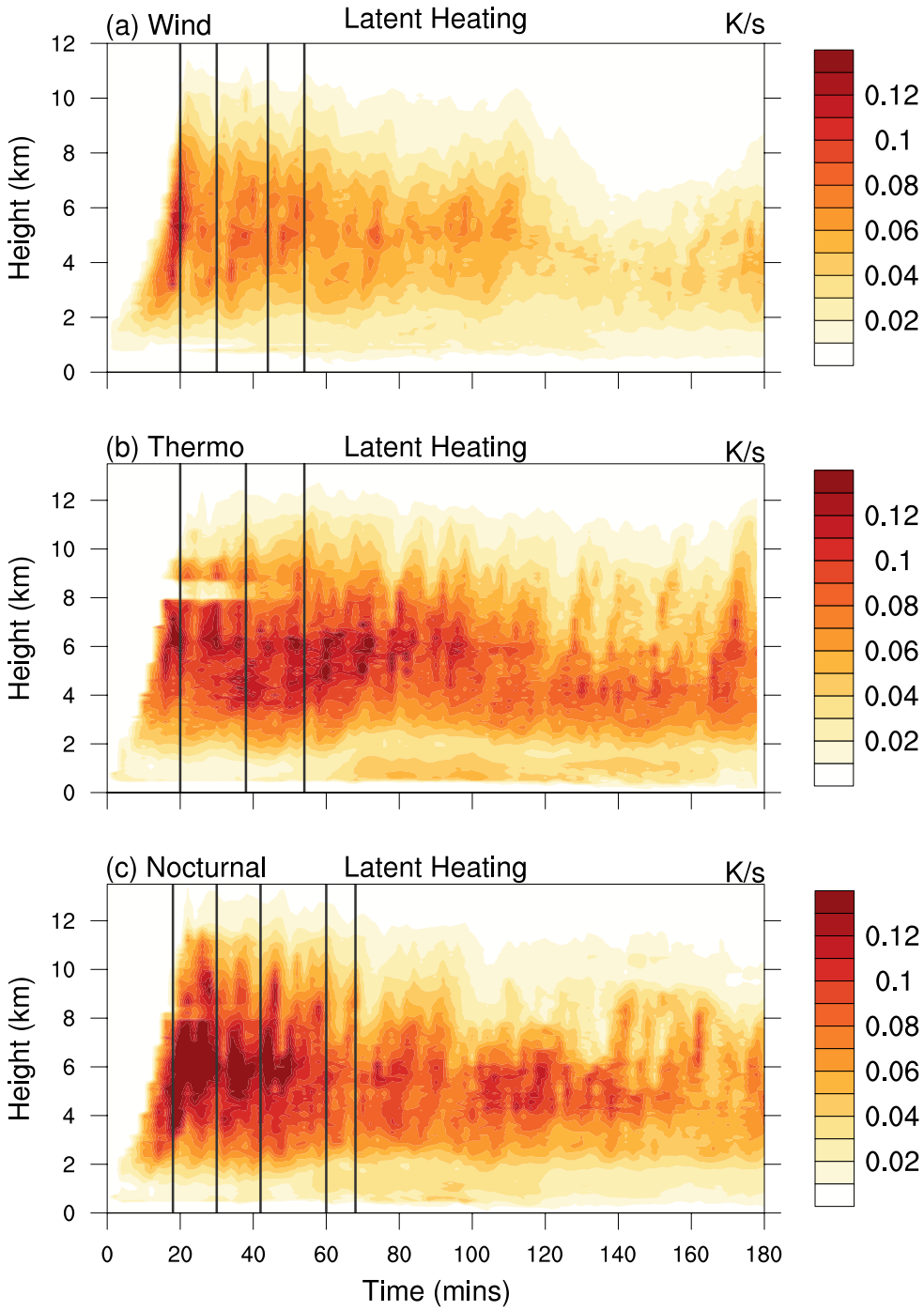

FIG. 4.4. As in Fig. 3.4 but for the (a) Wind, (b) Thermo, and (c) Nocturnal simulations and their respective N1 wave generation times as determined from Fig. 4.5.

4.1.1 N1 Gravity Wave Generation

As with the control simulation, the driver of N1 gravity wave generation in this simulation lies within the cellular nature of the updrafts and subsequent latent heat release. Fig. 4.4 (a) shows the

first four N1 wave generation times quickly following maximums in latent heat release over the depth of the storm. The four waves have been subjectively analyzed by the deep-tropospheric descent propagating away from the convection in Fig. 4.5 (a), but it is obvious from Fig. 4.4 (a) that the cyclical nature of latent heat release does not stop after the generation of those four waves.

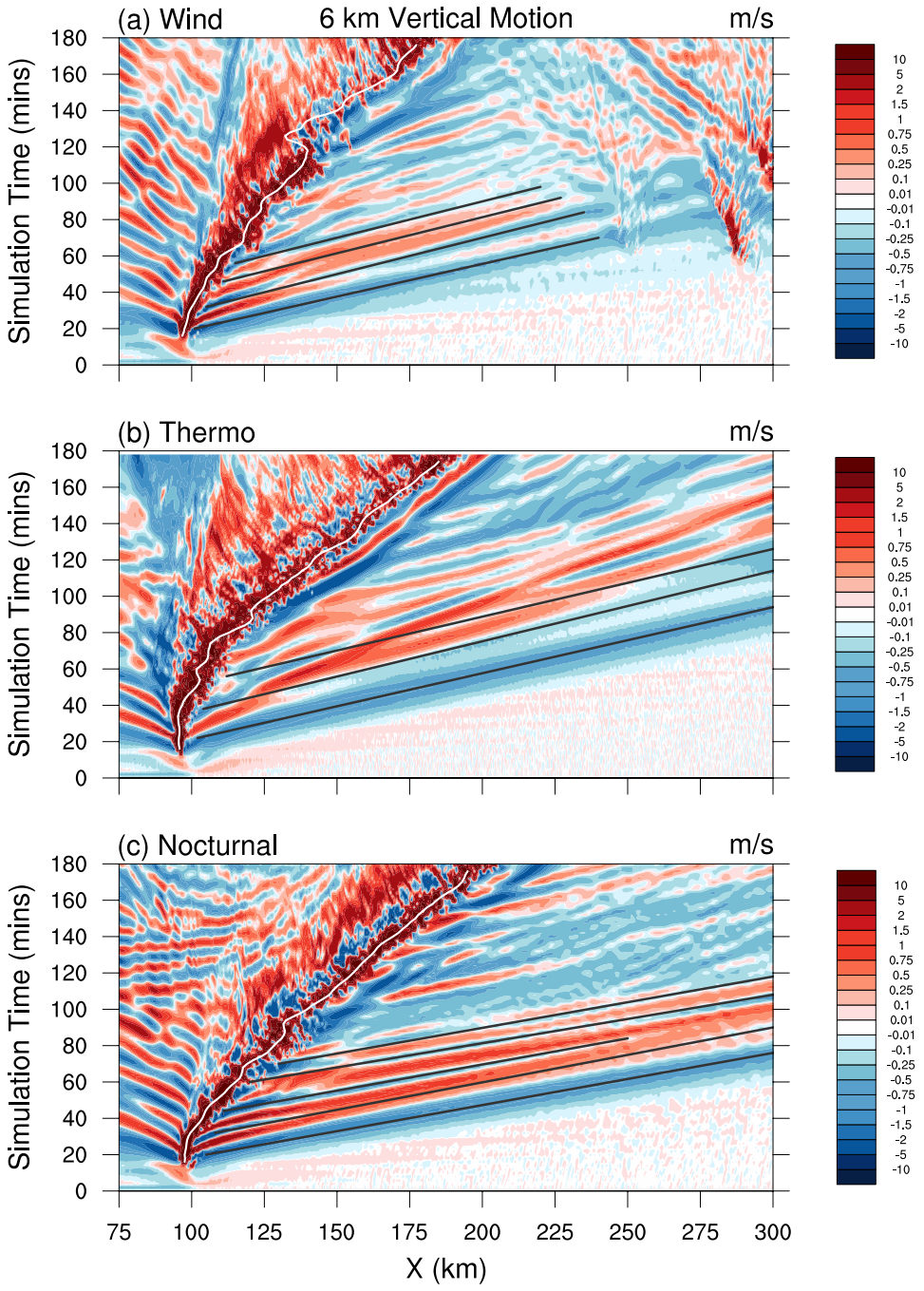

FIG. 4.5. As in Fig. 3.5 but for the (a) Wind, (b) Thermo, and (c) Nocturnal simulations and their respective N1 waves.

Spectral analysis is performed on the same three N1 gravity wave parameters, although in a slightly different manner than the control simulation in Section 3.3.1, to once again confirm gravity wave generation and influence beyond what can be subjectively identified. The analysis is performed over the same y domain cross section, however now only one spectrum is calculated over a time series derived from averaging together the 95^{th} percentile values of latent heating, updraft velocity, and pre-convective descent for each point within the cross section, giving 2 degrees of freedom. This method aids in reducing the noise within the time-series and highlighting the true processes occurring both within the MCS as well as the downstream environment. The resulting spectra can be found in Fig. 4.6 (a), where the 90% confidence limits have been adjusted accordingly to account for the 2 degrees of freedom. As in the control simulation, the three variables all have matching, significant spectra at 0.12 cycles/2 minutes, corresponding to N1 gravity wave generation and successive response downstream around every 17 minutes. The only difference between this simulation and the control is the introduction of deep layer shear. In response to this vertical wind profile, the MCS consistently has stronger updrafts and associated higher magnitudes of latent heat release. Even with this change to the internal dynamics of the system, the updrafts still show the same lifecycle period and remain the dominant factor in the generation frequency of these waves. This modified wind profile does not change the generation frequency of N1 gravity waves, only their strength.

4.1.2 N2 Gravity Wave Generation

While the timing of N1 waves depends largely on the cellularity of the updrafts, the signals for N2 gravity wave generation are not as clear and can differ greatly among the simulations. In the control simulation, the onset of precipitation to the surface generates the first N2 wave, but the same initial surge of cooling as hydrometeors fall below the melting level and cloud base is not enough to generate a N2 wave in this case. The control simulation's weak mid and upper level winds scarcely advect hail away from the convective line, concentrating the majority of latent cooling to this region at the start of the simulation. For the Wind simulation, stronger updrafts and mid to upper level storm relative winds result in hail remaining aloft above the melting level longer than in the control run. When precipitation first descends to the surface around 25 min, there is little cooling contribution from melting in the lower levels as seen in Fig. 4.7 (a) compared to the control simulation where melting extends to the surface with the onset of precipitation as seen in Fig. 3.8. Consequently, the magnitude of latent cooling over the lower levels at this time is not enough to generate an N2 wave. When fingers of reflectivity begin to extend from the convective line ahead of the storm around 35 minutes into the simulation, they

are accompanied by a surge of precipitation to the surface that includes hail and introduces additional cooling by melting in the lower levels outside of the downdraft. This increase and horizontal expansion of low-level cooling is enough to generate the first N2 wave shown by the increase in the rate of latent cooling in Fig. 4.7 (a) at this time as well as the quickly following low-level ascent shown by the first dashed line in Fig. 4.8 (a).

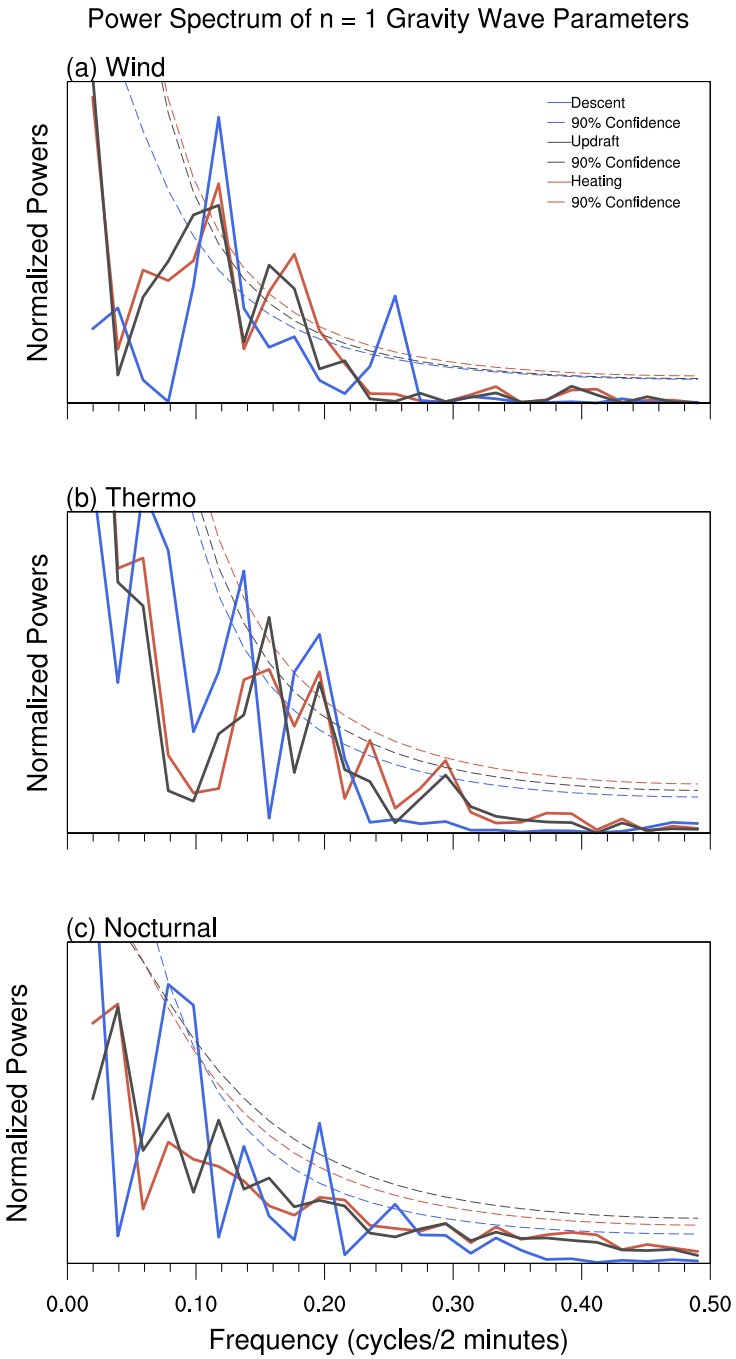

FIG. 4.6. As in Fig. 3.7 but for the (a) Wind, (b) Thermo, and (c) Nocturnal simulations.

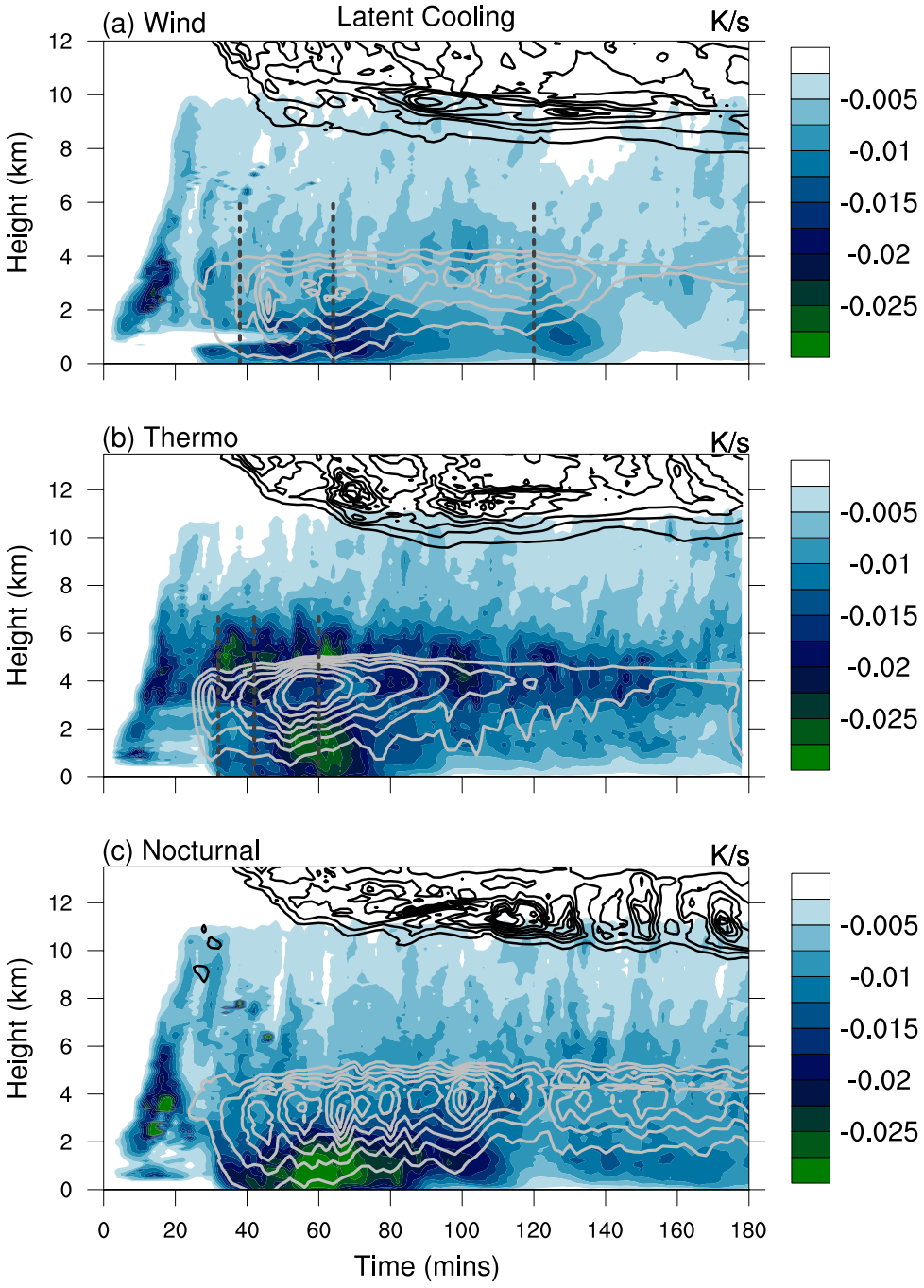

FIG. 4.7. As in Fig. 3.8 but for the (a) Wind, (b) Thermo, and (c) Nocturnal simulations and their respective N2 wave generation times as determined from Fig. 4.8. Note that the Nocturnal simulation does not have any analyzed N2 waves.

The next wave is generated just after 60 minutes into the simulation when a strong downdraft occurs within the MCS. Evaporational cooling below cloud base contributes to the generation of this wave, but there is also a large contribution of latent cooling from melting due to the increased amounts

of hail caught in the downdraft, and consequently the second N2 wave, indicated by the second dashed line in Fig. 4.7 (a), is generated. Finally, the last N2 wave analyzed in this simulation is generated when the storm begins to considerably weaken. The light blue line in Fig. 4.3 shows the updraft velocity as the storm progresses, and around 120 minutes into the simulation, the updraft almost completely ceases. This is the first sign of the collapse of the storm, and the weakened updraft is no longer able to suspend larger hydrometeors. As hail begins to descend through the storm, the values of latent cooling due to melting increase, and shortly thereafter, rates of evaporative cooling increase rapidly as the hydrometeors descend below cloud base to the surface as seen between 110 to 130 minutes in Fig. 4.7 (a). The large increase of latent cooling to the lower-levels in combination with the major decrease of latent heating in the mid to upper levels generates the final, considerably strong N2 wave.

4.1.3 Environmental Response

Considering the impacts the different initial wind profile has on the MCS, its latent heating profile, and the domain environment, the gravity waves also behave and propagate differently ahead of the system. Latent heating within this simulation is stronger in magnitude than the control simulation, which leads to stronger deep-tropospheric descent for the waves generated in response. Overall, the waves in this simulation are continually stronger than the same waves in the control simulation. The influence of the first two N1 waves is clear in Fig. 4.5 (a) in which their descent at 6 km can be seen throughout the entire domain even after interacting with single cell convection between 200 and 300 km. Although the waves are stronger in this simulation, their influence on the CAPE is consistent with that seen in the control simulation in which each N1 wave passage corresponds to a decrease in CAPE by 100 J kg^{-1} as shown in Fig. 4.9 (a).

The influence of N2 waves can often be compromised when overrun by N1 waves moving at twice the speed or lost within higher order wave modes, but the impacts that these waves have downstream are still significant. The passage of each N2 wave, shown by the dashed lines in Fig. 4.10, corresponds to a decrease in the LFC by at least 25 meters. In this environment, this factor leads to N2 waves aiding in the development of clouds ahead of the MCS. This influence can be seen with each of the three N2 waves in Fig. 4.8 (a), where the gray line contour represents the 0.01 g/kg cloud mixing ratio and the dashed lines are the three analyzed N2 waves. The clouds associated with the convection are drawn out with the N2 waves as they propagate away from the MCS. The clouds quickly retreat once downward motion from N1 waves and other processes act to suppress them, yet with the generation and propagation of another N2 wave, the clouds are drawn out once more.

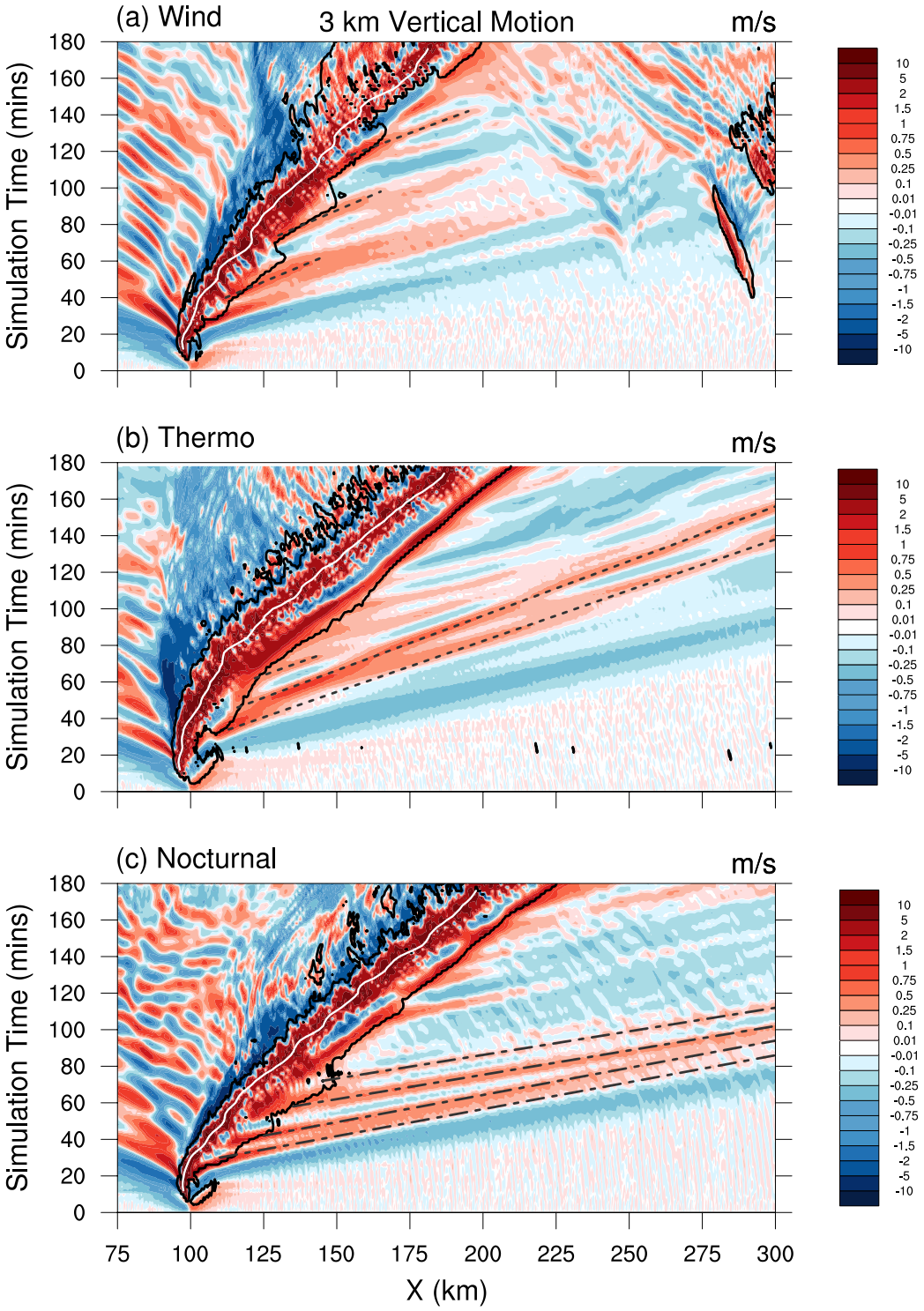

FIG. 4.8. As in Fig. 3.9 but for the N2 gravity waves in the (a) Wind and (b) Thermo simulations. The broken lines in (c) instead show the positive vertical motion components of N1 gravity waves in the Nocturnal simulation.

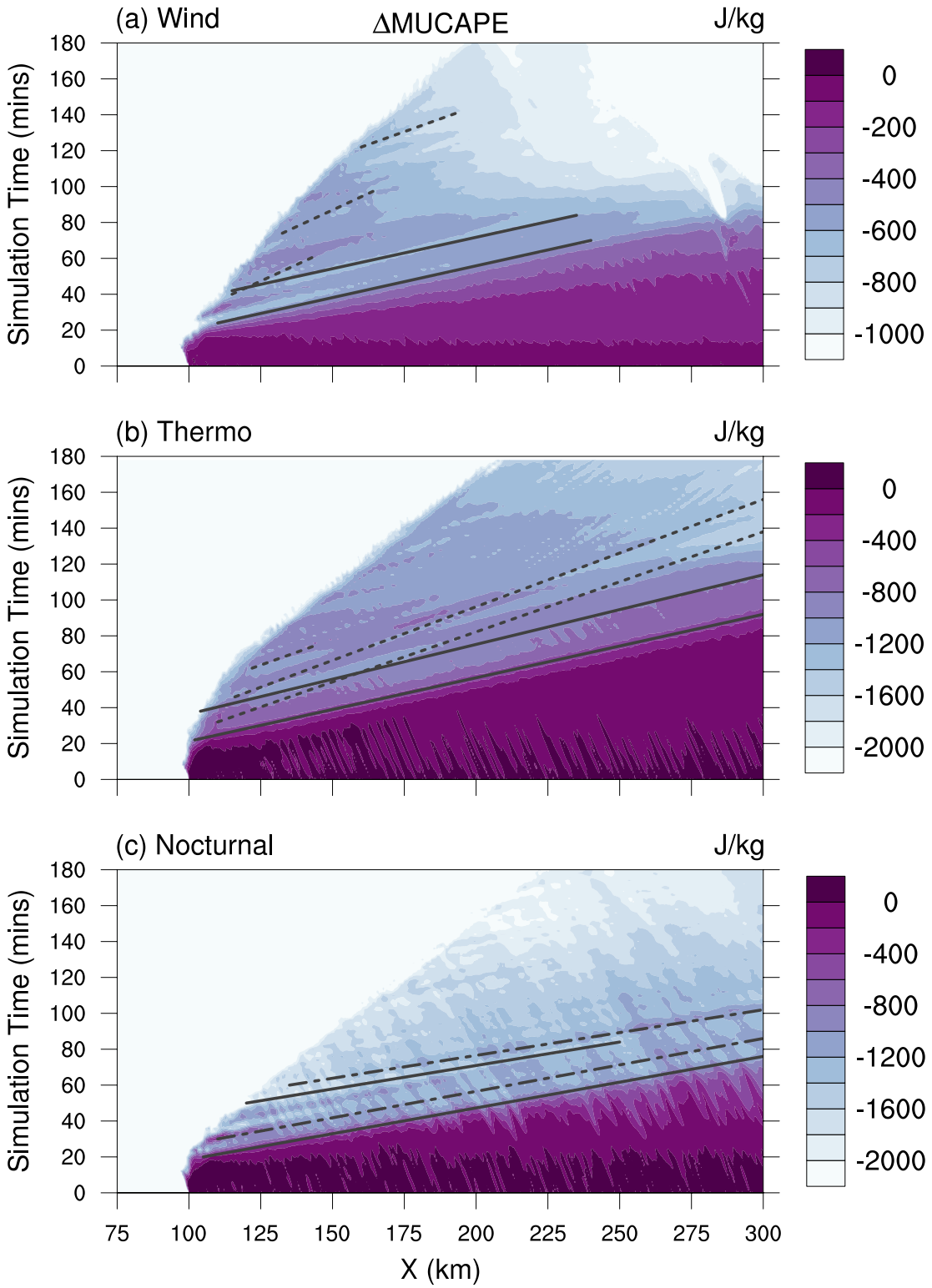

FIG. 4.9. As in Fig. 3.12 but for the N1 and N2 waves in the (a) Wind and (b) Thermo simulations. Changes in CAPE from the updraft/downdraft couplets of N1 waves for the Nocturnal simulation are shown in (c), where the broken lines indicate upward motion from the N1 waves.

Spurious convection first appears downstream of the MCS approximately 50 minutes into the simulation and continues for the duration of the run. While this new CI is not caused by low-frequency gravity waves, they still interact with the single cell storms, and the last N2 wave acts to re-invigorate one of the cells in its dissipation stage that is then quickly ingested by the MCS. As seen in Fig. 4.11 (a), 100 minutes into the simulation, the MCS is strong, well organized and catching up to a convective single cell approximately 50 km ahead. A dense concentration of hail lofted well into the upper levels shows the strength and vertical extent of the thriving MCS updrafts, and the intensity and horizontal extent of the rain are the greatest seen in the entire simulation. The cell downstream has begun to precipitate and even has a small presence of hail within the storm as it progresses into its mature stage at this time. Just over 20 minutes later, both the MCS and the single convective cell have weakened significantly as manifested in 4.11 (b) by the notable decrease in hydrometeors. The last N2 wave is generated around this time by the surge of latent cooling due to the rapid evaporation and melting of hydrometeors shown in Fig. 4.7 (a) as they can no longer remain suspended by the significantly weakened updraft of the MCS. This wave and its associated low-level ascent propagate away from the MCS at about 20.6 m s^{-1}, decreasing the LFC by at least 25-50 meters as shown by the last dashed line in Fig. 4.10. When this wave interacts with the remnants of the decayed cell, the low-level ascent and increased relative humidity that accompanies the wave quickly revives the cell just before 136 minutes into the simulation as shown in Fig. 4.11 (c). Within minutes, the cell is further strengthened when it interacts with the vertical motion associated with the cold pool. When the cell is absorbed by the MCS, the additional buoyancy it brings into the system revives the MCS and strengthens the updrafts along the convective line (Fig. 4.3), a process also seen in Fovell et al. (2006) and Adams-Selin and Johnson (2013). A distinct, strong updraft signal can be seen at the leading edge of the convection by 166 minutes into the simulation by lofted values of cloud ice and hail as shown in Fig. 4.11 (d).

The N2 wave directly assists in the resurgence of the MCS by reviving the single convective cell that is quickly absorbed, resulting in a discrete propagation episode of the convective line. These results are very similar to those seen in Fovell et al. (2006), however the key difference between these mechanisms is that the new cell is not generated by high-frequency waves as in that study but instead by model noise. Regardless, the N2 wave has a direct impact on the single cell that aids in reinvigorating the MCS. This is an exciting result that not only further supports how cell absorption can have a vastly positive influence on the system, but also that N2 waves are capable of strengthening and reviving cells downstream as well.

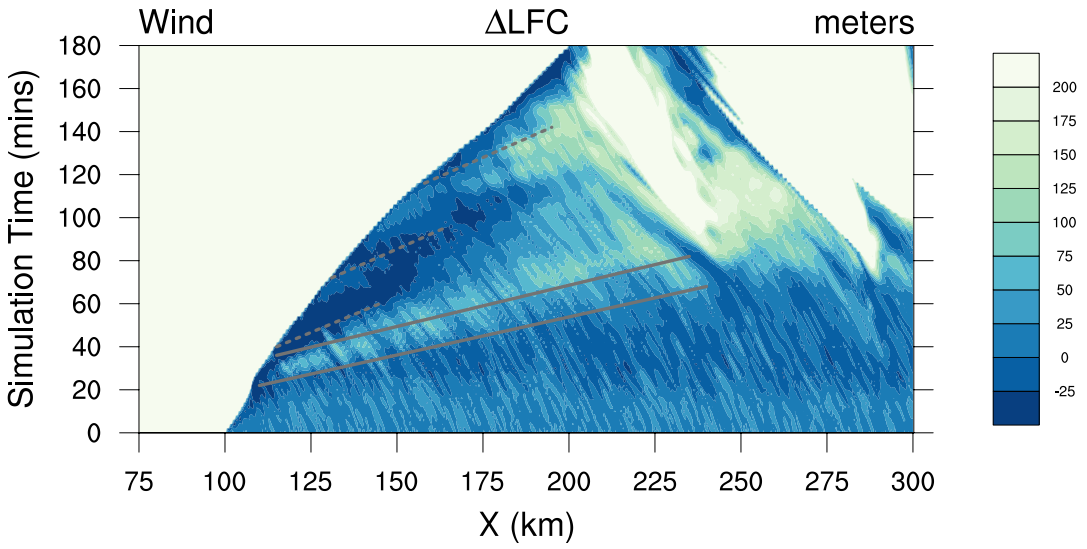

FIG. 4.10. As in Fig. 3.13 but for the Wind simulation and associated N1 and N2 waves.

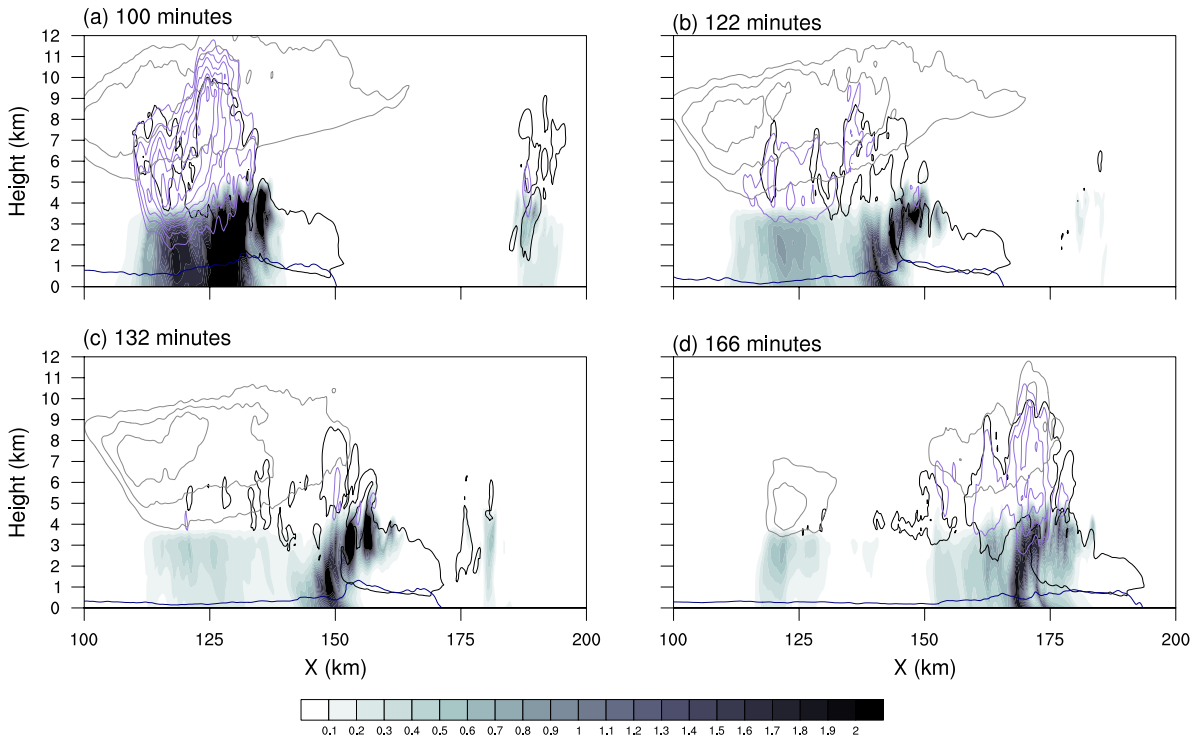

FIG. 4.11. Vertical cross sections of the hydrometeor composition of the MCS and downstream single convective cell at (a) 100 minutes, (b) 122 minutes, (c) 132 minutes, and (d) 166 minutes into the Wind simulation. The blue contour shows the location of the cold pool, the purple line contours represent q_g from 0.5 to 5 by 0.5, the black contour is the q_c at 0.15, the gray contours are q_i from 0 to 4 by 1, and filled color contours show q_r, all in g kg^{-1}. Note: the y axis domain was changed for this figure alone to a 10 km box centered about y = 90 km to capture the ingestion of the single cell.

4.2 Nocturnal Thermodynamic Environment

The environment used to initialize this simulation utilizes the same idealized wind shear profile as the control simulation, however the thermodynamic profile is a slightly modified version of the nocturnal PECAN profile detailed in Chapter 2. The input sounding for this simulation is shown in Fig. 4.12. Though the nocturnal boundary layer is just under 100 mb deep, the stable layer introduces enough convective inhibition (CIN) to generally hinder surface parcels, rendering the convection elevated just as the MCS sampled in PECAN. Parcels that are able reach the LFC (located around 1360 meters) have access to large amounts of elevated MUCAPE, emphasizing the importance and influence that N2 waves, which aid in lifting parcels, can have.

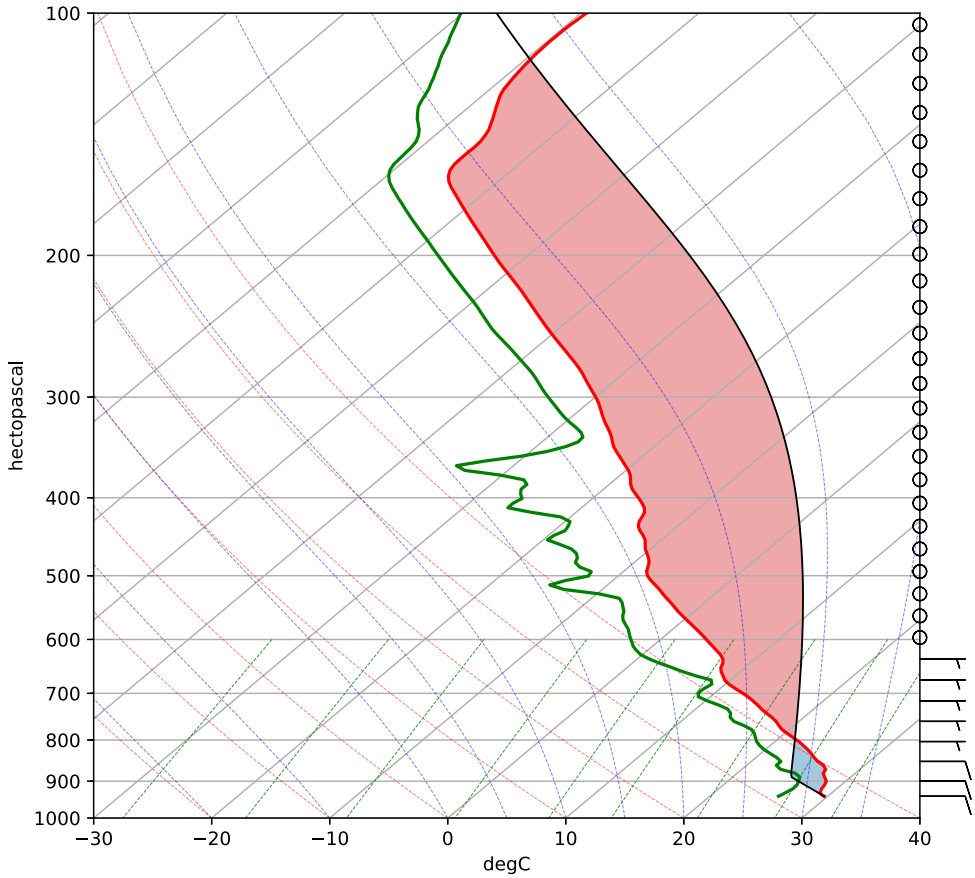

FIG. 4.12. As in Fig. 3.1 but for the input sounding used to initialize the Thermo simulation. The blue shaded region indicates CIN in J kg^{-1}.

Although they have vastly different thermodynamic profiles, there are no drastic structural changes between this MCS and the MCS in the control simulation. Both MCSs exhibit "fingers" of reflectivity

as seen in Fig. 4.2 (a) and (c), but the MCS within this simulation is the only one to have them periodically throughout the duration of the run, indicating the persistent presence of a moist absolutely unstable layer (Bryan et al. 2007). The intensity of this system far exceeds that of the control simulation, with overshooting tops reaching beyond the tropopause at 13.7 km for the first 100 minutes of the simulation, speaking to the strength and resilience of the updrafts shown by the green line in Fig. 4.3. Although both MCSs demonstrate some degree of bowing, the process occurs rapidly within this case, and as a result, the storm relative velocity drastically increases just after 30 minutes into the simulation. The slope of the white lines representing the location of maximum updraft speed at 3 km and 6 km in Figs. 4.5 (b) and 4.8 (b) show the rapid increase in speed at this time.

4.2.1 N1 Gravity Wave Generation

Considering the influential changes to the thermodynamic environment between the control simulation and this run, it is to be expected that significant differences between the updrafts and latent heating profiles within this MCS would follow, in turn influencing the timing and strength to which N1 gravity waves are generated. Of pivotal importance to note is that the tropopause is now located around 13.7 km instead of 12 km as in the control and Wind simulations, elongating the vertical column, deepening the potential extent to which latent heating can occur, and increasing the theoretical N1 gravity wave speed to 48 m s^{-1} by Eq. (1.1) with a mean column N of 0.011 s^{-1}. Also, while layers of absolute instability (negative N) have been removed from the input sounding per CM1 requirements, new trapping levels are introduced with this thermodynamic profile, allowing examination of gravity wave generation and propagation within a more realistic nocturnal environment.

Although the MCS produced from this environment has the same general life cycle and structure as the MCS in the control simulation, their vertical latent heating profiles differ greatly as the systems develop. As shown in Fig. 3.4, the heating profile for the control simulation is consistent with gravity wave theory in which the rates of maximum latent heating occur directly in the middle of the troposphere (6 km in the control simulation; Nicholls et al. 1991). However, Fig. 4.4 (b) shows that the maximum in latent heating in this simulation is a bit more shallow, with maximum rates also occurring around 6 km but within an environment where the tropopause is at 13.7 km. The rates of latent heat release approach almost twice that of the rates that generated N1 waves in the control simulation, indicating that the downstream influence of these waves should also be stronger. The gap in latent heating rates between 8 and 9 km for the first 40-50 minutes of the simulation is due to spurious clouds forming at

that level throughout the domain that act to skew the 95^{th} percentile values of latent heating towards smaller rates.

Spectral analysis becomes increasingly useful in identifying N1 waves as the MCSs and pre-convective environment become more complicated with the complex thermodynamic initialization profile. The objectively analysis was applied again to the 95^{th} percentile time-series of updraft velocity (similar to that shown in Fig. 4.3), latent heat release, and descent ahead of the convection in the same manner as Section 4.1.1. Each have significant spectra around 0.20 cycles/2 minutes as seen in Fig. 4.6 (b). This corresponds to signals for gravity wave generation as well as downstream influence around every 10 minutes. Maximums in latent heat release rates can be subjectively identified with this kind of frequency in Fig. 4.4 (b), but the corresponding gravity wave signature of deep tropospheric descent appears to be half as frequent in Fig. 4.5 (b). Results from the spectral analysis performed on this simulation indicate that there are likely more N1 gravity waves being generated and traveling downstream than can be easily subjectively identified, and that the introduction of this nocturnal thermodynamic environment changes the frequency of updraft development cycles and N1 generation. Compared to the frequency of 0.12 cycles/2 minutes for the simulations using the modified Weisman and Klemp (1982) thermodynamic profile, this nocturnal environment has increased sensitivity to changes within the latent heating profile and has created more active cellularity in the updrafts, and subsequently more N1 waves are generated in response.

4.2.2 N2 Gravity Wave Generation

Although the microphysical warming profiles initially differed greatly between this simulation and the control run, the latent cooling structure within this MCS, as seen in Fig. 4.7 (b), is remarkably similar to that in the control simulation (Fig. 3.8). The structure of latent cooling due to melting shows obvious similarities, where high rates of evaporation are also occurring in the mid-levels as apposed to the wind simulation where the majority of evaporation occurs below cloud base. The N2 gravity wave generation mechanisms are also similar between this simulation and the control. The first wave is generated just after the onset of precipitation to the surface, and as the storm begins to mature as evidenced by the development of a trailing stratiform region, another wave is generated around 40 minutes into the simulation as the horizontal extent of cooling expands. 20 minutes later, rapidly increasing rates of latent cooling with contributions from both evaporation and melting are observed as a strong downdraft occurs within the storm, generating the last analyzed wave of the simulation.

4.2.3 Environmental Response

In spite of the fact that the magnitude of latent heating within this simulation is almost twice that of the control simulation, the consequent descent from the N1 waves, highlighted by the solid gray lines in Fig. 4.5 (b), is only slightly stronger. While the first N1 wave acts to decrease the magnitude of MUCAPE by over 200 J kg^{-1} for the entire domain, shown by the first gray line in Fig. 4.9 (b), the second wave's influence is fleeting once it interacts with the first N2 wave of the simulation. The N2 wave is generated with the onset of precipitation to the surface with similar rates of evaporative cooling that generated the first N2 wave in the control run. However, the latent cooling rates due to melting are much higher within this simulation at this time, and so the first N2 wave and its associated ascent are also much stronger (Fig. 3.9 and Fig. 4.8). While the ascent from this wave travels throughout the entire domain, its positive influence on the MUCAPE field stops once it interacts with the N1 wave. The second N2 wave, generated as a result of the broadening horizontal extent of latent cooling as the stratiform region develops, has the greatest downstream influence as its associated ascent is the strongest and farthest reaching out of any of the N2 waves in either the control or Thermo simulations. This wave helps to increase the MUCAPE by 200 J kg^{-1}, counteracting the reduction by a previous N1 wave. The final N2 wave of the simulation, generated by a strong downdraft within the MCS, has a limited impact as the environment ahead of the MCS becomes increasingly chaotic.

4.3 Nocturnal Environment

The sounding used for this simulation, shown in Fig 4.13, incorporates the vertical wind profile used in the Wind simulation as well as the same thermodynamic profile used in the Thermo simulation. This input sounding emulates a true nocturnal environment featuring a LLJ, veering winds, and a nocturnal boundary layer. Despite the 20% relative humidity addition within the lowest 200 mb, the MCS generated within this environment is remarkably similar to the observed MCS from PECAN from which the environment was sampled. Fig. 4.14 shows a range height indicator (RHI) scan taken from the S-band/Ka-band dual polarization, dual wavelength doppler radar deployed during the field campaign (see Hubbert et al. 2018 for more details on the radar observations taken during PECAN). At 0607 UTC, the radar was located approximately 25 km to the south-east of the MCS, offering an insight to the internal structure of the system. For comparison, a vertical cross-section of radar reflectivity of the mature, simulated MCS is shown Fig. 4.15. Both MCSs consist of multiple convective cells with stronger cells at the leading edge of the system and older cells advected rearward due to the storm inflow. The

reflectivity of the simulated MCS is not only realistic but also matches well with the observed MCS, and both MCSs have a convective region where the consistent horizontal extent of reflectivity greater than 45 DBZ is around 40 kms. While the past three simulations have been valuable to learn the sensitivities of gravity waves to wind shear and nocturnal environments, this simulation will act to best represent the gravity wave activity that may have been occurring during the mature period of the actual MCS sampled during PECAN.

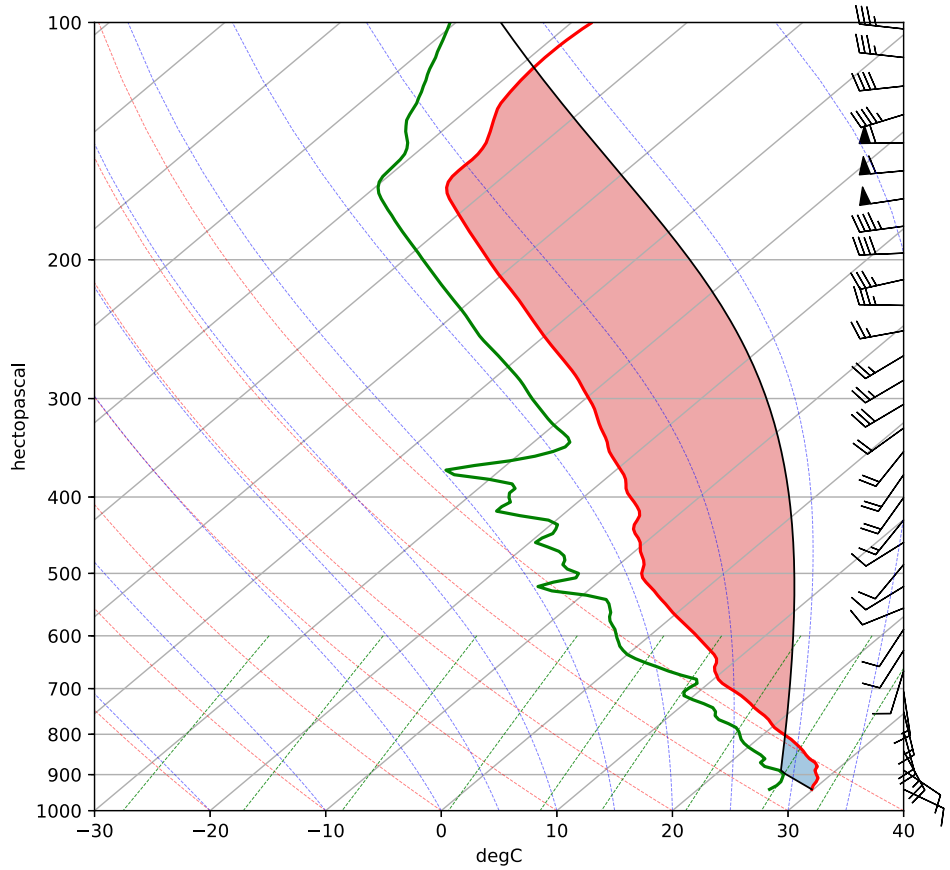

FIG. 4.13. As in Fig. 4.12, but for the input sounding used to initialize the Nocturnal simulation.

As to be expected, the resulting MCS mimics aspects of both the Wind and Thermo simulations. The extent of the stratiform region is modest compared to that of the control and Thermo simulations as well as the actual observed MCS, a characteristic only shared with the Wind simulation (Fig. 4.2 (b)). This indicates that vertical wind shear plays an important role in the development (or lack thereof) of the stratiform region, and subsequently also in the structure of latent cooling and N2 gravity wave generation. However, the strength and speed of the system imitates that of the Thermo simulation MCS. By every parameter, this is the strongest MCS out of all the simulations, and this characteristic is

blatantly apparent compared to the updraft time-series of the other simulations in Fig. 4.3. The rates of latent heating (Fig. 4.4 (c)) and cooling (Fig. 4.7 (c)) are also the strongest, and thus so are the vertical motions downstream associated with each wave mode.

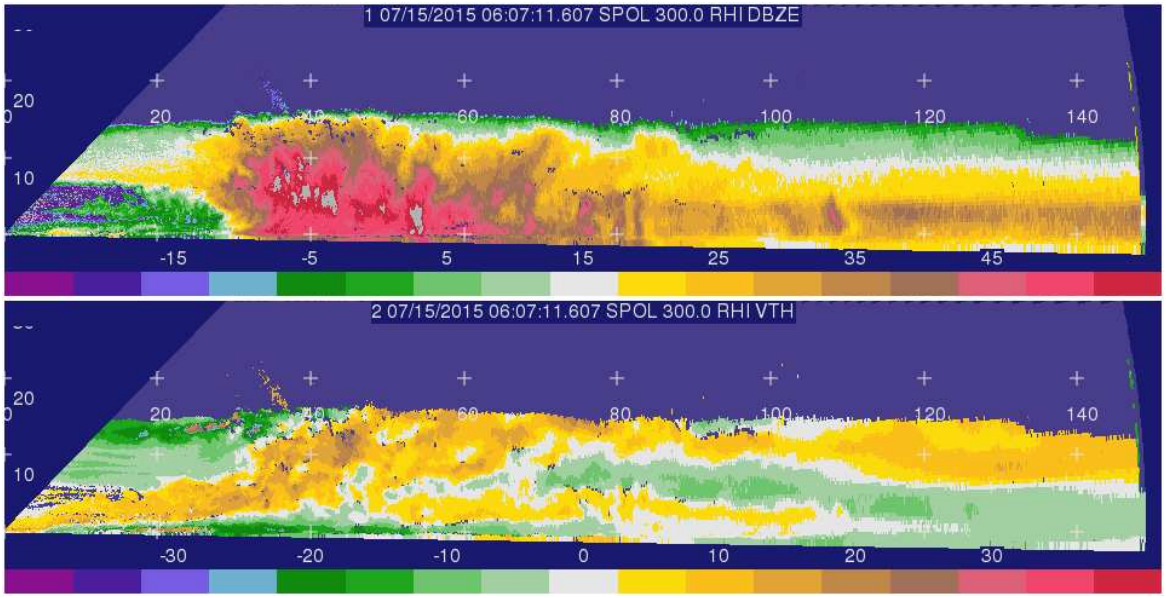

FIG. 4.14. A RHI scan of the observed PECAN MCS at 0607 UTC. The top panel shows the radar reflectivity and the lower panel the velocity, with respective magnitudes on the bottom of each panel. The numbers on the y and x axes of the panels delineate the height and distance in km from the radar respectively.

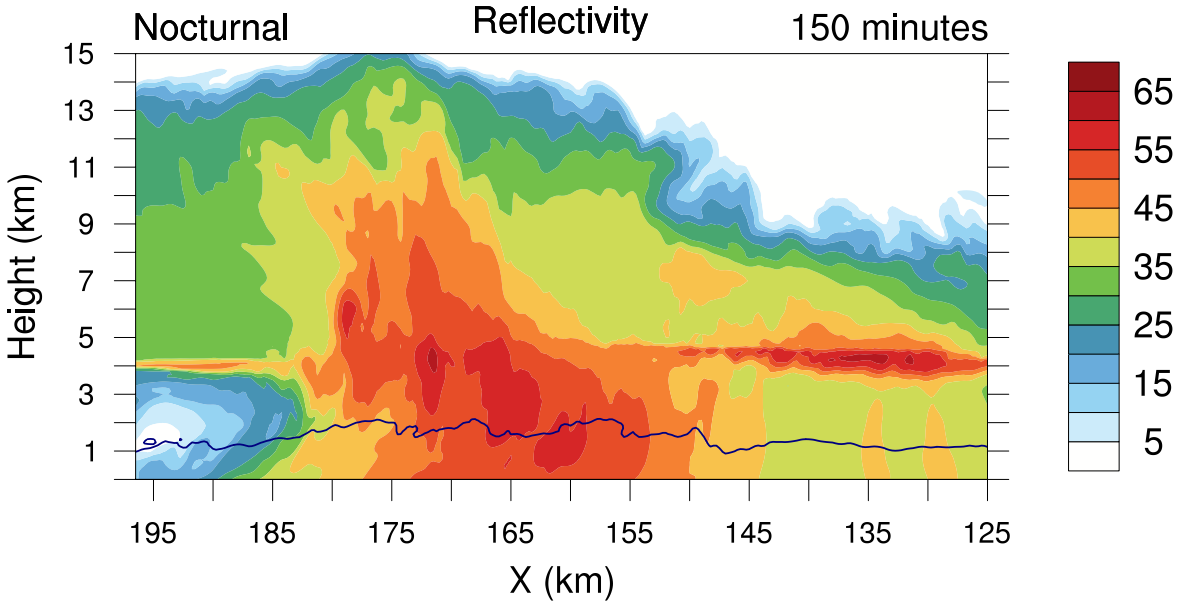

FIG. 4.15. Vertical cross section of reflectivity of the mature simulated MCS with the X axis reversed to match the orientation of the RHI scan in Fig. 4.14. The navy contour delineates the cold pool.

4.3.1 *Gravity Wave Generation*

Consistent with the other simulations, fluctuations in the intensity of latent heat release solely determine the frequency and strength of the N1 waves, and the rates of microphysical heating within this MCS are sometimes over double that of the control simulation (Figs. 3.4 and 4.4 (c)). Spectral analysis of the N1 gravity wave parameters shown in Fig. 4.6 (c) reveals a significant spectral peak of N1 gravity wave descent at a frequency of 0.20 cycles/2 minutes, the same frequency of descent as in the Thermo simulation. The activity within this MCS conceals any signal of updraft cycling and latent heat fluctuations within the spectral analysis, rendering a direct comparison of N1 gravity wave generation to updraft cycling unfeasible. Unique to this simulation is the presence of strong, easily identifiable periods of deep-tropospheric ascent immediately following the descent of the N1 waves. Previous studies have found that as the rates of microphysical heating subside temporarily during updraft cycling, a wave of upward motion throughout the depth of the troposphere propagates away from the MCS in response (e.g. Nicholls et al. 1991; Lane and Zhang 2011; Adams-Selin and Johnson 2013). While this process is true within all of the simulations, the response waves in this simulation are the only ones to have a notable impact downstream.

The structure of latent cooling within this MCS mimics that of the wind simulation, where strong evaporative cooling is reserved for the lowest levels as opposed to the control and thermodynamic simulations in which there are large amounts of evaporative cooling around the freezing level as well. Quite opposite from the wind simulation, however, is the production and downstream influence of N2 waves. From Fig. 4.8 (c), the periods of ascent at 3 km, denoted by the broken lines, are actually caused by the upward motion couplet of the N1 waves and are not associated with N2 waves. While N2 waves could very easily be hidden among the wave motions of these couplets as well as other higher order wave modes, there is no subjective way to identify them. Even though the rates of latent cooling are substantial, it is not enough to generate strong, distinguishable N2 waves in this case.

4.3.2 *Environmental Response*

The descent associated with the N1 waves can be seen in Fig. 4.5 (c). The waves are moving rapidly at a speed of 53.4 m s^{-1}, just over the theoretical speed of 50 m s^{-1} calculated by Eq. (1.1) after removing the mean tropospheric zonal wind of 5.14 m s^{-1}. As seen in the other simulations, the downward motion associated with these waves acts to dry and warm the column, decreasing MUCAPE with each wave passage (Fig. 4.9 (c)). The strong upward motions associated with the N1 couplets are generally

difficult to distinguish, which is why they have not been discussed in the previous simulations. However in this simulation, not only are they strong and easily identifiable, but the ascent from these waves is substantial enough to also be recognized in the lower levels, shown by the broken lines in Fig. 4.8 (c). While not always as strong as the upward motion associated with N2 waves in the other simulations, the ascent is significant enough to aid in new cloud development ahead of the convection with each wave passage. As seen in Fig. 4.9 (c), the upward vertical motion associated with the negative N1 waves also aids in MUCAPE restoration, where each broken line immediately following the solid lines acts to counteract the MUCAPE reduction that the positive N1 waves created as theorized in McAnelly et al. (1997). Su and Zhai (2017) observed similarly strong N1 wave couplets within their case study that aided in CI. It is also possible that concealed N2 waves could be aiding in these processes as well, but since they are not easily identifiable, the influence of any N2 waves is inconclusive.

CHAPTER 5

DISCUSSION AND CONCLUSIONS

Low-frequency gravity waves have been previously largely studied in the context of daytime and tropical MCSs, and only limited work has addressed the generation mechanisms and impacts of these waves in environments more suitable for mid-latitude MCSs. To connect N1 gravity wave generation from fluctuations in the latent heating profile to updraft cyclicity, as well as to examine the potential of low-frequency gravity waves to support or suppress new and existing convection, four idealized cloud model simulations are conducted to address these objectives within environments with complex vertical wind shear and nocturnal thermodynamic characteristics. Each simulation introduces considerable changes to the generated MCS that alter not only the internal dynamics of the system but also the way in which the low-frequency waves are generated and impact the downstream environment.

These objectives are first tested within a highly idealized environment. Spectral analysis is utilized to confirm the mechanism behind N1 gravity wave generation through fluctuations within the latent heating profile but also to extend this generation mechanism to the concurrent cyclical nature of the MCS updrafts. The 95^{th} percentile values of updraft velocity, latent heat release, and pre-convective descent all between 5 to 8 km are examined for this analysis and reveal that within this highly idealized environment, all three variables fluctuate at the same frequency of 0.12 cycles/2 minutes. This corresponds to the updraft velocity and latent heating rates having cyclical re-development approximately every 17 minutes, and perturbations of mid-level descent far ahead of the convective line occur at the same rate. These results strongly suggest that N1 waves and associated periods of deep-tropospheric descent over 100 km ahead of the MCS are generated by variations within the latent heating profile due to the cellular nature of MCS updrafts.

What differs among the simulations regarding N1 waves is their general strength and frequency. The Wind simulation, which has slightly stronger updrafts and increased rates of latent heating compared to the control simulation, has identical frequencies among the N1 gravity wave parameters as the control simulation. The impact of wind shear within this environment does not change the updraft redevelopment frequency but only their strength, and the forward environment experiences the same frequency of N1 gravity waves albeit stronger than the same waves in the control run due to the increased rates of latent heating. The Thermo simulation, however, displays much more frequent cyclical redevelopment of the updrafts. When spectral analysis is performed on the 95^{th} percentile values

of updraft velocity, latent heating rates, and pre-convective descent, the results also show matching spectra for these three variables but at a higher frequency, with perturbations occurring approximately every 10 minutes. The introduction of the nocturnal environment, which has remarkably stronger initial CAPE compared to the control and Wind simulations, acts to increase the cellular redevelopment frequency of the system and subsequently also increases the frequency of fluctuations in the latent heating profile and gravity wave generation. Regardless of their frequency, the N1 waves share a similar influence downstream within all of the simulations in which the passage of each wave reduces the CAPE and occasionally acts to also increase the LFC.

The generation mechanisms and environmental influence of the N2 gravity waves vary among the simulations considerably more than the N1 waves. Three waves are analyzed within the control simulation which are generated in response to surges in latent cooling with contributions from both melting and evaporation. The generation of the first N2 wave occurs when rain and hail descend to the surface at the start of the simulation, and the second, stronger wave is generated when the horizontal expanse of latent cooling is increased due to the development of a trailing stratiform region. Although their thermodynamic profiles are vastly different, the Thermo simulation and the control run share a very similar structure of latent cooling and N2 wave generation mechanisms. The rates of latent cooling are much stronger in the Thermo simulation, however, and therefore so is the low-level ascent associated with the N2 waves ahead of the MCS. Within these simulations, there are strong rates of evaporative cooling at the melting level that only descend to the surface with increased hydrometeor fallout often seen within strong downdrafts. The control and Thermo simulations share the same idealized vertical wind profile, implying that in environments with little upper-level wind shear atop more pronounced shear below, N2 gravity wave generation mechanisms are consistent among daytime and nocturnal MCSs.

The control and Wind simulations share the same thermodynamic environment yet the structure of latent cooling is vastly different. Evaporative cooling within the control simulation is well distributed among the lower half of the troposphere with the strongest rates of latent cooling occurring around the melting level. This simulation's lack of wind shear in the mid to upper levels in combination with weaker updraft velocities prevents prolonged hail suspension, and with the first downdraft, both rain and hail descend to the surface and contribute to a strong latent cooling surge in the lower half of the troposphere. The Wind simulation, however, confines the majority of evaporative cooling to below cloud base. The deeper wind shear and stronger updrafts act to suspend hail within the convection

for longer, and consequently the first onset of precipitation to the surface lacks latent cooling due to melting hydrometeors and therefore lacks the latent cooling response needed to initiate an N2 wave at this time. This requirement is true among all of the simulations; N2 waves are only generated when surges in both melting and evaporation occur.

The Nocturnal simulation is an outlier to the rest in many ways. Numerous studies have detailed how N1 waves can have both deep-tropospheric descent and ascent components (e.g. Nicholls et al. 1991; McAnelly et al. 1997) which are well demonstrated within this simulation. The descent component is generated in response to increases in latent heat release as previously mentioned, however when the latent heat release decreases as part of the cyclical development, the ascent portion of the N1 wave is generated. The vertical motion associated with this part of the N1 wave is often small and difficult to ascertain when concealed by more impactful waves, however in this case, the updraft couplet is strong and easily distinguishable. Also unique to this simulation is the lack of any discernible N2 waves. Even though the values of latent cooling are the strongest among all of the simulations, it is still not enough to generate strong, discernible N2 waves. Although no N2 waves are able to be subjectively identified, the cloud development ahead of the MCS is likely a result of juxtaposed ascent contributions from both concealed N2 waves and the updraft component of the N1 waves.

Overall, the generation mechanism of N1 gravity waves can be directly linked through spectral analysis to fluctuations within the latent heating profile that occur as a result of the cellular redevelopment of MCS updrafts. The Control and Wind simulations show cyclicity in these variables at the same frequency, implying that vertical wind shear does not impact the redevelopment frequency of daytime MCS updrafts and associated N1 wave generation. However, the introduction of a nocturnal environment acts to increase the cellularity of the updrafts, subsequently increasing the frequency of N1 gravity waves. N2 gravity wave generation mechanisms are essentially identical among daytime and nocturnal MCSs in environments where the majority of wind shear is confined to the lower levels, however surges in both melting and evaporation are required to create a substantial latent cooling response enough for generation. Within environments with deep vertical wind shear, the destabilization that the ascent associated with low-frequency gravity waves provides can aid in cloud development ahead of the MCS as well sustain and support convection downstream.

This work truly underscores the importance of proper and representative parameterization of microphysical processes and associated latent heating within not only these idealized cloud models but also in numerical weather prediction (NWP) in order to more accurately resolve the frequency, strength,

and timing of low-frequency gravity waves. Applying these findings to NWP and observational analysis fosters a more accurate representation of the impacts these waves may have on convective favorability around MCSs. Further comprehension of low-frequency gravity wave dynamics can improve our understanding of environmental factors that could support potential convection initiation and cloud development far beyond the parent MCS. These results also beg the question: do low-frequency gravity waves play a larger role in MCS maintenance than previously thought?

Nocturnal convection remains an evolving area of study highly dependent upon environmental characteristics, and the impact that low-frequency gravity waves may have on MCS maintenance should be a factor considered in future studies. The Nocturnal simulation represents one of the many MCSs documented during the PECAN field campaign, and applying the results from this study to the observations from the mission in which the environment was initialized from can potentially aid in identifying any low-frequency gravity waves, their paths, and their impacts on the environment surrounding the MCS. Future work should consider additional simulations with nocturnal mid-latitude environmental characteristics to establish a foundation of low-frequency gravity wave dynamics within these representative mid-latitude environments to more accurately realize their application to NWP and observational analysis. Soundings from other PECAN missions are available to serve as initialization environments to create similar idealized simulations in which the findings could be directly applied to a network of high-resolution observations in order to further study the dynamics behind low-frequency gravity waves and their potential feedback on the parent system.

REFERENCES

Adams-Selin, R. D., 2019: Impact of convectively-generated low-frequency gravity waves on evolution of a mesoscale convective system. *J. Atmos. Sci.*, submitted.

Adams-Selin, R. D. and R. H. Johnson, 2013: Examination of gravity waves associated with the 13 March 2003 bow echo. *Mon. Wea. Rev.*, **141 (11)**, 3735–3756, doi: 10.1175/MWR-D-12-00343.1.

Bryan, G. H. and J. M. Fritsch, 2002: A benchmark simulation for moist nonhydrostatic numerical models. *Mon. Wea. Rev.*, **130 (12)**, 2917–2928, doi: 10.1175/1520-0493(2002)130<2917:ABSFMN>2.0.CO;2.

Bryan, G. H., R. Rotunno, and J. M. Fritsch, 2007: Roll circulations in the convective region of a simulated squall line. *J. Atmos. Sci.*, **64 (4)**, 1249–1266, doi: 10.1175/JAS3899.1.

Fovell, R. G., 2002: Upstream influence of numerically simulated squall-line storms. *Quart. J. Roy. Meteor. Soc.*, **128 (581)**, 893–912, doi: 10.1256/0035900021643737.

Fovell, R. G., G. L. Mullendore, and S.-H. Kim, 2006: Discrete propagation in numerically simulated nocturnal squall lines. *Mon. Wea. Rev.*, **134 (12)**, 3735–3752, doi: 10.1175/MWR3268.1.

French, A. J. and M. D. Parker, 2010: The response of simulated nocturnal convective systems to a developing low-level jet. *J. Atmos. Sci.*, **67 (10)**, 3384–3408, doi: 10.1175/2010JAS3329.1.

Gallus, W. A. and R. H. Johnson, 1991: Heat and moisture budgets of an intense midlatitude squall line. *J. Atmos. Sci.*, **48 (1)**, 122–146, doi: 10.1175/1520-0469(1991)048<0122:HAMBOA>2.0.CO;2.

Geerts, B., et al., 2017: The 2015 Plains Elevated Convection at Night Field Project. *Bull. Amer. Meteor. Soc.*, **98 (4)**, 767–786, doi: 10.1175/BAMS-D-15-00257.1.

Houze, R. A., 2004: Mesoscale convective systems. *Rev. Geophys.*, **42 (4)**, doi: 10.1029/2004RG000150.

Hubbert, J. C., J. W. Wilson, T. M. Weckwerth, S. M. Ellis, M. Dixon, and E. Loew, 2018: S-Pol's polarimetric data reveal detailed storm features (and insect behavior). *Bull. Amer. Meteor. Soc.*, **99 (10)**, 2045–2060, doi: 10.1175/BAMS-D-17-0317.1.

Lane, T. P. and M. J. Reeder, 2001: Convectively generated gravity waves and their effect on the cloud environment. *J. Atmos. Sci.*, **58 (16)**, 2427–2440, doi: 10.1175/1520-0469(2001)058<2427:CGGWAT>2.0.CO;2.

Lane, T. P. and F. Zhang, 2011: Coupling between gravity waves and tropical convection at mesoscales. *J. Atmos. Sci.*, **68 (11)**, 2582–2598, doi: 10.1175/2011JAS3577.1.

Mapes, B. E., 1993: Gregarious tropical convection. *J. Atmos. Sci.*, **50 (13)**, 2026–2037, doi: doi.org/10.1175/1520-0469(1993)050<2026:GTC>2.0.CO;2.

McAnelly, R. L., J. E. Nachamkin, W. R. Cotton, and M. E. Nicholls, 1997: Upscale evolution of MCSs: Doppler radar analysis and analytical investigation. *Mon. Wea. Rev.*, **125 (6)**, 1083–1110, doi: 10.1175/1520-0493(1997)125<1083:UEOMDR>2.0.CO;2.

Morrison, H., G. Thompson, and V. Tatarskii, 2009: Impact of cloud microphysics on the development of trailing stratiform precipitation in a simulated squall line: Comparison of one-and two-moment schemes. *Mon. Wea. Rev.*, **137 (3)**, 991–1007, doi: 10.1175/2008MWR2556.1.

Naylor, J. and M. S. Gilmore, 2012: Convective initiation in an idealized cloud model using an updraft nudging technique. *Mon. Wea. Rev.*, **140 (11)**, 3699–3705, doi: 10.1175/MWR-D-12-00163.1.

Nicholls, M. E., R. A. Pielke, and W. R. Cotton, 1991: Thermally forced gravity waves in an atmosphere at rest. *J. Atmos. Sci.*, **48 (16)**, 1869–1884, doi: 10.1175/1520-0469(1991)048<1869:TFGWIA>2.0.CO;2.

Pandya, R., D. Durran, and C. Bretherton, 1993: Comments on "Thermally forced gravity waves in an atmosphere at rest". *J. Atmos. Sci.*, **50 (24)**, 4097–4101, doi: 10.1175/1520-0469(1993)050<4097:COFGWI>2.0.CO;2.

Peters, J. M. and R. S. Schumacher, 2016: Dynamics governing a simulated mesoscale convective system with a training convective line. *J. Atmos. Sci.*, **73 (7)**, 2643–2664, doi: 10.1175/JAS-D-15-0199.1.

Rotunno, R., J. B. Klemp, and M. L. Weisman, 1988: A theory for strong, long-lived squall lines. *J. Atmos. Sci.*, **45 (3)**, 463–485, doi: 10.1175/1520-0469(1988)045<0463:ATFSLL>2.0.CO;2.

Schmidt, J. M. and W. R. Cotton, 1990: Interactions between upper and lower tropospheric gravity waves on squall line structure and maintenance. *J. Atmos. Sci.*, **47 (10)**, 1205–1222, doi: 10.1175/1520-0469(1990)047<1205:IBUALT>2.0.CO;2.

Schumacher, R. S., 2009: Mechanisms for quasi-stationary behavior in simulated heavy-rain-producing convective systems. *J. Atmos. Sci.*, **66 (6)**, 1543–1568, doi: 10.1175/2008JAS2856.1.

Schumacher, R. S., 2015: Sensitivity of precipitation accumulation in elevated convective systems to small changes in low-level moisture. *J. Atmos. Sci.*, **72 (6)**, 2507–2524, doi: 10.1175/JAS-D-14-0389.1.

Skamarock, W. C., 2004: Evaluating mesoscale NWP models using kinetic energy spectra. *Mon. Wea. Rev.*, **132 (12)**, 3019–3032, doi: 10.1175/MWR2830.1.

Su, T. and G. Zhai, 2017: The role of convectively generated gravity waves on convective initiation: A case study. *Mon. Wea. Rev.*, **145 (1)**, 335–359, doi: 10.1175/MWR-D-16-0196.1.

Trapp, R. J. and J. M. Woznicki, 2017: Convectively induced stabilizations and subsequent recovery with supercell thunderstorms during the mesoscale predictability experiment (MPEX). *Mon. Wea. Rev.*, **145 (5)**, 1739–1754, doi: 10.1175/MWR-D-16-0266.1.

Weisman, M. L. and J. B. Klemp, 1982: The dependence of numerically simulated convective storms on vertical wind shear and buoyancy. *Mon. Wea. Rev.*, **110 (6)**, 504–520, doi: 10.1175/1520-0493(1982)110<0504:TDONSC>2.0.CO;2.

Weisman, M. L., W. C. Skamarock, and J. B. Klemp, 1997: The resolution dependence of explicitly modeled convective systems. *Mon. Wea. Rev.*, **125 (4)**, 527–548, doi: 10.1175/1520-0493(1997)125<0527:TRDOEM>2.0.CO;2.

Wilson, J., S. Trier, D. Reif, R. Roberts, and T. Weckwerth, 2018: Nocturnal elevated convection initiation of the PECAN 4 July hailstorm. *Mon. Wea. Rev.*, **146 (1)**, 243–262, doi: 10.1175/MWR-D-17-0176.1.